American Mineralogist, Volume 81, pages 284–302, 1996

Molecular dynamics simulations of liquids and glasses in the system $NaAlSiO_4$-SiO_2: Physical properties and transport mechanisms

D.J. Stein and F.J. Spera

Department of Geological Sciences and Institute for Crustal Studies, University of California, Santa Barbara, California 93106, U.S.A.

Abstract

Thermodynamic and transport properties of ten compositions in the binary system $NaAlSiO_4$-SiO_2 have been determined by the method of molecular dynamics simulation. The computations were performed on collections of 1300 particles at temperatures between 2500 and 4500 K and pressures of 4 ± 1.5 GPa using a pairwise-additive potential energy function with Coulombic and Born-Mayer interactions. Results are presented for both thermodynamic and transport properties; compositional patterns in the computed properties are considered in relation to structural information, such as nearest-neighbor and second-nearest-neighbor coordination and intertetrahedral angle distributions (see Stein and Spera 1995). Heat-capacity values extrapolate to within 0.25R of those found in laboratory measurements in the range 1000–1800 K, and estimates of compressibility and expansivity agree with available data within a factor of two to four. Transport properties are computed by time-correlation statistics from configuration histories between 0.04 and 0.09 ns in duration, and results are presented for ionic conductivity and self-diffusivity. For the charge-balancing cation Na, diffusivity displays Arrhenian variation from 2×10^{-5} cm²/s to 1×10^{-4} cm²/s. These results extrapolate with fair success into the thermal regime of experimental measurements. For network formers O, Si, and Al, diffusivity varies from about 2×10^{-8} cm²/s for SiO_2-rich compositions at 2500 K to 2×10^{-6} cm²/s for $NaAlSiO_4$ at 4500 K. For all ions, diffusivity tends to increase along isotherms with addition of $NaAlO_2$ to SiO_2, but activation energy shows no systematic compositional variation.

Diffusive activation energy for network formers (averaging 128, 118, and 140 kJ/mol for Al, Si, and O, respectively) displays neither the magnitude nor compositional variability anticipated from application of the Stokes-Einstein or Eyring relations to extensive viscometric data for this compositional series. Analysis shows that in the ranges of temperature, density, and duration of the present series of experiments, a critical transition occurs in the O diffusion mechanism, from continuous network reorganization at high temperatures to discrete hops by a few mobile particles between static sites at low temperatures. Simulation temperatures lie mostly below a critical transition region postulated in mode-coupling theory for condensed matter, and bulk network diffusivity under these conditions is relatively uninformative regarding processes of viscous flow. Aspects of the transition are explored by using the statistics of individual particle displacements, using the van Hove density-autocorrelation function, and studying the trajectories of individually tagged particles. Analysis of the frequency of site exchange among a subpopulation of mobile O ions gives results more consistent with extrapolated values of viscosity at these temperatures. The apparent Arrhenian activation energy of the site-exchange process is similar to that measured for viscous flow and shows the requisite compositional variation identified in viscometric studies.

Studies in which the dependence of the critical temperature of the ergodic-to-nonergodic transition is studied as a function of pressure and composition have the potential to shed additional light on the relation between silicate melt structure and dynamics on the atomic scale.

Introduction

Coupled viscous flow and diffusion processes play a major role in the transport of energy and material within magma bodies and within the Earth as a whole. O occupies an essential structural and volumetrically dominant position in mineral and melt phases of the crust and mantle, and numerous laboratory measurements of O diffusivity in silicates appear in the materials science literature

0003–004X/96/0304–0284$05.00

(Oishi et al. 1975; Yinnon and Cooper 1980; Kalen et al. 1991). Additional work has addressed diffusion of O and network-forming cations in geochemically relevant compositions (Dunn 1982; Kushiro 1983; Shimizu and Kushiro 1984; Wendlandt 1991; Rubie et al. 1993). Numerous recent NMR spectroscopic measurements have focused on detecting the structures and time scales involved in diffusion of network-forming species in silicates (Liu et al. 1987, 1988; Farnan and Stebbins 1990, 1994; Stebbins et al. 1992).

The technique of molecular dynamics (MD) simulation provides detailed information about the positions and motions of atoms in the liquid state and is capable of elucidating transport mechanisms in silicate melts. MD studies of silicates and their analogs have emphasized the diffusion rates of network-forming species, the description of liquid structures related to diffusive events, and the relation of diffusion to viscous flow (Brawer 1981; Soules and Busbey 1981; Rustad et al. 1990; Kubicki and Lasaga 1990). An influential viewpoint has been that of Brawer (1985) regarding the role of a varying concentration of anomalously coordinated "defect" sites in explaining changes of diffusivity (or viscosity) with temperature and composition.

This is the second part of a two-part molecular dynamics simulation study of the variation with pressure, temperature, and composition of structural, thermodynamic, and transport properties in continuous-network silicate glasses and melts in the system $NaAlSiO_4$-SiO_2. Results were obtained in constant-volume (NVE) ensembles of 1300 particles for ten compositions and simulation durations between 0.04 and 0.1 ns using a simple pairwise-additive model of the interatomic potential energy. For temperatures between 2500 and 4500 K, densities in the primary MD cell of 2300–2400 kg/m^3 yield pressures of 5 GPa or less. Details of the simulation methodology are presented in Stein and Spera (1995) along with a description of the melt structures obtained from the simulations and comparisons with results of diffraction experiments (e.g., nearest- and second-nearest-neighbor coordination, pair-correlation and radial-distribution functions, and bonding angle distributions).

Here, we continue by discussing thermodynamic and transport properties observed in the simulations and relate their variation with composition to systematic changes in structure. The first of two major objectives of this work is to measure the success of simple pair potentials in recovering various material properties of molten silicates by making comparisons with available laboratory measurements. Thermodynamic properties presented in this study include heat capacity, compressibility and thermal expansivity, and the equation of state for compositions studied polythermally. Transport properties to be discussed are the coefficients of self-diffusivity for all species and ionic conductivity.

O transport governs processes of viscous flow in network melts (e.g., Brawer 1985), and results for O are emphasized in discussion of properties obtained in the simulations. The Stokes-Einstein or Eyring relations (see below) are typically applied to O self-diffusivity data to predict melt viscosity. However, it is the kinetics of the most mobile O ions in the simulations that successfully accounts for extrapolations of viscosity variation measured in the laboratory (Stein and Spera 1993). Not surprisingly, the transport of Na, approximately two orders of magnitude more rapid than that of O, Si, and Al, accounts almost entirely for the ionic conductivity.

Molecular dynamics simulations are well suited to probing subnanosecond relaxation processes in dense fluids. This regime encompasses a transition in the dynamics of the liquid from an ergodic state in which all or most ions are mobile to one exhibiting broken ergodicity characterized by activated jumps between local minima on the potential energy surface (Goldstein 1969; Angell 1988, 1991; Stillinger 1995). When this transition is complete, structural rearrangement in the liquid is effectively frustrated by the requirements of cooperative dynamics, i.e., that the motion of individual particles is hindered by "cages" formed by surrounding particles. This transition is thought to occur generally in the viscosity range of 1–1000 Pa·s and is quite distinct from the phenomenological glass transition at 10^{12} Pa·s, defined by macroscopic relaxation times (10^3–10^4 s). The latter involves measurable changes in static thermodynamic properties, such as the isochoric heat capacity, whereas the former does not. Determination of the critical temperature of the ergodicity-breaking transition is a key outcome of recent developments in the description of microscopic dynamics of dense liquids (Hansen and McDonald 1986) by means of nonlinear mode–coupling theory (Bengtzelius et al. 1984; Leutheusser 1984; Kim and Mazenko 1992). Certain correlation functions easily obtainable from the results of MD simulations (e.g., the van Hove density-autocorrelation and intermediate-scattering functions) are capable of illuminating this transition, and it has been observed in simulations of fluids with quite diverse models of the interparticle potential energy. The second principal objective of the present study is to illustrate aspects of this transition for a model of a relatively structured, "strong" network silicate liquid and to clarify the conditions under which it is possible to link viscous flow to network diffusivity through phenomenological relations such as the Stokes-Einstein equation.

Thermodynamic properties and equation of state

The isochoric heat capacity (C_V) and the equation of state were extracted from the MD results for each composition. As described in the first part of this study, compositional variation was accomplished by an idealized isoelectronic substitution of $Na^+ + Al^{3+}$ for Si^{4+} along the compositional join SiO_2-$NaAlSiO_4$; compositions are indicated by the mole percent of $NaAlSiO_4$ component, e.g., $NaAlSi_2O_6$ is designated N50, etc. Almost all simulations were performed in the microcanonical ensemble (NVE, constant volume, mass, and energy). To compute

TABLE 1. Internal energy

	ρ	2500 K	3000 K	3500 K	4000 K
N20	2264	−3908	−3894	−3881	−3870
N33	2263	−3731	−3718	−3704	−3693
N41	2274	−3639	−3625	−3612	−3599
N50	2289	−3545	−3531	−3521	−3507
N53	2249				−3474
N57	2249				−3438
N60	2261	−3457	−3443	−3433	−3415
N63	2249				−3395
N66	2249				−3364
N100	2367	−3201	−3185	−3174	−3158

Note: Energy given in kilojoules per gram-atom for NVE simulations; fluctuation in energy is approximately 0.03 kJ/(g-atom); density (ρ) given in kilograms per cubic meter.

compressibility and thermal expansivity, several additional simulations in the isothermal-isobaric (NPT) ensemble were performed for N33, N50, and N100 at 3000 K and pressures of 2.8 or 4 GPa, depending on composition, using velocity and coordinate-scaling techniques (Berendsen et al. 1984).

Heat capacity

Internal energy of each NVE composition and temperature is reported in Table 1. In general, for temperatures in the range of 2500–4000 K, kinetic energy was approximately 0.7–1% of the total internal energy, and energy fluctuations were approximately 1 part in 10^5. During each NVE simulation, the heat capacity was computed according to

$$C_V = N\mathrm{k}[N - N\mathrm{k}T\langle E_\mathrm{k}^{-1}\rangle(\tfrac{3}{2}N - 1)]^{-1} \qquad (1)$$

(Haile 1992), where $\langle E_\mathrm{k}^{-1}\rangle$ is approximated by the time average of the reciprocal of the kinetic energy during the simulation, and temperature is defined in terms of the average kinetic energy during the simulation $T = (\tfrac{3}{2}N\mathrm{k})^{-1}\langle E_\mathrm{k}\rangle$.

Figure 1a shows the variation of heat capacity with temperature for the compositions SiO_2, N33, N50, and N100 and compares the MD results to calorimetric measurements by Richet and Bottinga (1984). Anharmonicity in crystals increases C_V above 3R, or 24.9 J/(K·g-atom) near the melting temperature, and contributions to communal entropy arising from network rearrangement result in some additional increases of C_V in the liquid state. However, linear extrapolation of the results of Richet and Bottinga to ~3000 K is not reasonable for strong network liquids such as those of the present study. Extrapolation of the MD results to the median temperature of the laboratory data gives values near 3R, generally lower than the laboratory measurements on supercooled liquids by 0.25R and showing little compositional variation.

Coincidentally, the magnitude of the discrepancies shown in the above comparison is of the same order as the increase in heat capacity at the calorimetric glass transition. The explanation of the discrepancies may be related to the fact that for some of the compositions, the

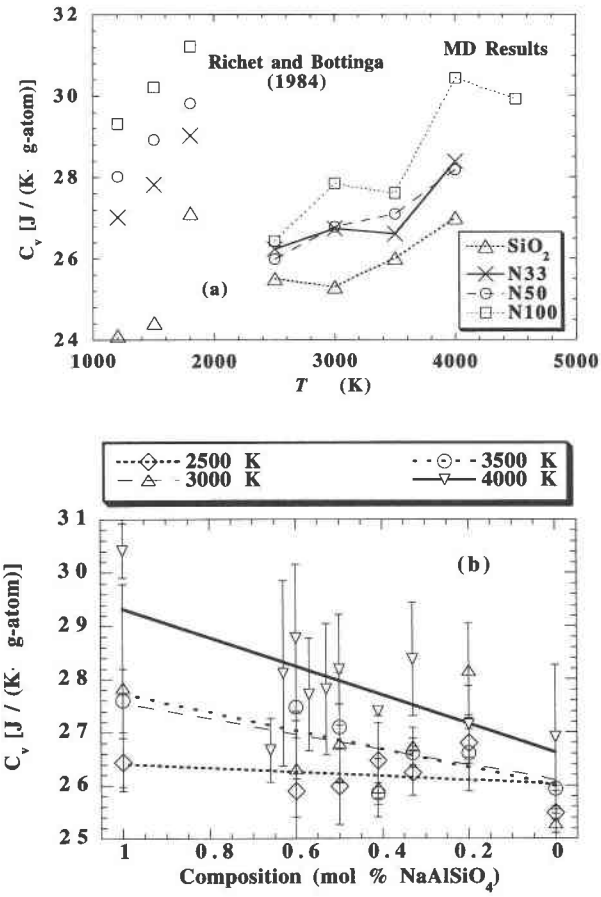

FIGURE 1. (**a**) Variation of constant-volume heat capacity with temperature, on a gram-atom basis. Results of thermochemical measurements for the liquid in the range 1100–1800 K by Richet and Bottinga (1984) are included for reference. (Note that results of Richet and Bottinga for SiO_2 span the glass-transition region.) Triangles = N00, SiO_2; Xs = N33, $NaAlSi_3O_8$; circles = N50, $NaAlSi_2O_6$; and squares = N100, $NaAlSiO_4$. (**b**) Variation of constant-volume heat capacity with composition at four simulation temperatures. Symbols represent averages of two to five experimental segments of 10 ps or greater; error bars represent 1σ sampling uncertainties.

transition from ergodic to nonergodic behavior as revealed by the MD results (see below) occurs at temperatures at the upper end of the range of the data, i.e., between about 3500 and 4000 K. Hence, most heat-capacity values computed in the present study were determined for liquids that are effectively frozen on the experimental time scale, whereas the laboratory measurements of liquid-C_P were obtained under ergodic conditions. In theory, thermal effects of this magnitude are not expected to accompany the ergodic to nonergodic transition in MD studies (e.g., Wahnstrom 1991). We therefore conclude that limitations inherent in the form of the interatomic potential energy expression account (at least in part) for the apparent overestimates of dC_V/dT (and consequent underestimates of supercooled liquid heat capacity).

TABLE 2. Heat capacity at constant volume

	ρ	2500 K	3000 K	3500 K	4000 K
SiO_2	2251	25.48 ± 0.12	25.29 ± 0.18	25.94 ± 0.05	26.91 ± 1.36
N20	2264	26.79 ± 0.27	28.16 ± 0.89	26.61 ± 0.72	27.14 ± 0.73
N33	2263	26.24 ± 0.42	26.74 ± 0.35	26.61 ± 0.27	28.38 ± 1.07
N41	2274	26.47 ± 0.71	25.96 ± 0.55	25.85 ± 0.21	27.40 ± 0.09
N50	2289	25.99 ± 0.72	26.79 ± 0.745	27.10 ± 1.03	28.18 ± 1.04
N53	2249				27.81 ± 1.24
N57	2249				27.72 ± 1.06
N60	2261	25.90 ± 1.01	26.32 ± 0.91	27.47 ± 1.35	28.77 ± 1.38
N63	2249				28.11 ± 1.74
N66	2249				26.67 ± 0.60
N100	2367	26.44 ± 0.46	27.84 ± 1.95	27.60 ± 0.60	30.42 ± 0.51

Note: C_V in joules per kelvin-gram-atom; density (ρ) in kilograms per cubic meter.

Estimates of C_V from the slope of the energy-temperature relationship give values (interpolated at 3250 K) of 25.6, 24.8, and 28.0 J/(K·g-atom) for N33, N50, and N100, respectively. Figure 1b indicates that C_V increases regularly with decreasing concentration of SiO_2 component at all temperatures, agreeing qualitatively with the results of Richet and Bottinga (1984). The compositional variation obtained by Richet and Bottinga at about 1800 K is similar to that shown by the simulation results at 4000 K.

Heat capacity at constant pressure is related to C_V by

$$C_P = C_V + \frac{\alpha_P^2 VT}{\beta_T} \tag{2}$$

given in terms of molar volume (V), temperature (T), and isobaric expansivity (α_P) and isothermal compressibility (β_T) defined with respect to density (ρ) as follows: $\alpha_P = (-1/\rho)(\partial\rho/\partial T)_P$ and $\beta_T = (1/\rho)(\partial\rho/\partial P)_T$. At 3000 K for $NaAlSi_3O_8$, the correction amounts to 0.001R (significantly less than the representative uncertainty for any single composition and temperature of about 0.1R). Results for pure SiO_2 were also obtained over the range from 2500 to 4000 K, showing negligible variation with temperature and yielding a value of 25.8 ± 0.9 J/(K·g-atom) (see Table 2 and Fig. 1b). Richet and Bottinga (1984) measured C_P at just over 27 J/(K·g-atom) for amorphous silica above the glass transition, a discrepancy of 0.15R.

Equation of state

The simulations were performed at constant volume for each composition, in all cases approximating the densities of glasses prepared at 100 kPa. Thus, as the temperature of the simulation was modified, pressure in the cell varied, giving the equation of state for each composition. Equation-of-state (EOS) results for the NVE simulations are presented in Table 3. On the basis of least-squares fitting of time-averaged (P-T) pairs, the value of $(\partial P/\partial T)_V$ (equivalent to the ratio α_P/β_T) varies from approximately 0.3 MPa/K for composition N20 to more than 1.2 MPa/K for $NaAlSiO_4$. Little variation appears for intermediate compositions, with a $(\partial P/\partial T)_V$ value of approximately 0.6 MPa/K for N33–N60.

Isothermal compressibility and thermal expansivity

For the compositions N33, N50, and N100, β_T was found by performing independent simulations in the NPT ensemble (constant pressure of 4 GPa for N33 and N100, and 2.8 GPa for N50 at a temperature of 3000 K for each of the three compositions). The relation

$$\beta_T = \frac{1}{VkT}\langle \delta V^2 \rangle \tag{3}$$

was used to compute β_T, where $\langle \delta V^2 \rangle$ represents the time-averaged, mean-squared volume fluctuation, $\langle V \rangle^2$-$\langle V^2 \rangle$, in the NPT ensemble (Allen and Tildesley 1987). Values obtained for N33 were 4.1×10^{-12} Pa^{-1} and 3.85×10^{-12} Pa^{-1}; the value of α_P calculated from the EOS obtained at constant volume is therefore $\sim 2.3 \times 10^{-6}$ K^{-1}. Results for the three compositions are summarized in Table 4. In addition, correction of simulation results for β_T was made with estimates of the temperature derivative of β_T in the liquid and the pressure derivative of β_T for crystalline albite as referenced by Kress et al. (1988). This calculation resulted in a value of 1.6×10^{-11} Pa^{-1} extrapolated to 1373 K and 100 kPa, in comparison with the β_T value of 5.78×10^{-11} Pa^{-1} published by Kress et al. (1988). Decreases in sodium aluminosilicate compressibility with decreasing silica content were inferred by Kress et al. (1988) to result from the increasing occurrence of small (hence, less flexible) intertetrahedral

TABLE 3. Equation of state from polythermal simulations (NVE)

	ρ	P_0 (bar)	$(\partial P/\partial T)_V$ (bar/K)	R^2
N20	2264	32800	2.97	0.45
N33	2263	22100	5.55	0.66
N41	2274	16600	7.45	0.85
N50	2289	15800	6.33	0.67
N60	2261	13800	5.80	0.69
N100	2367	1350	12.30	0.94

Note: Fluctuations in pressure and temperature: $\sigma_P \approx 0.6$–0.7 GPa; $\sigma_T \approx$ 40–60 K; EOS parameters from least-squares regression of (T-P) pairs. The correlation coefficient for the P-T relationship is given by R^2.

TABLE 4. Compressibility and thermal expansivity

Composition	N33a	N33b	N50	N100
$\langle P \rangle$ (GPa)	4.0	4.0	2.8	4.0
$\langle T \rangle$ (K)	3000	3000	3000	3040
Isothermal compressibility (Pa^{-1})	4.09×10^{-12}	3.85×10^{-12}	4.73×10^{-12}	4.77×10^{-12}
$(\partial P/\partial T)_v$ (Pa/K)	5.55×10^{5}	5.55×10^{5}	6.33×10^{5}	1.23×10^{6}
Isobaric expansivity (K^{-1})	2.27×10^{-6}	2.14×10^{-6}	2.99×10^{-6}	5.87×10^{-6}

bond angles associated with the substitution of Al in tetrahedral sites in the liquid, a structural tendency described in Stein and Spera (1995), which is consistent with earlier spectroscopic results (Taylor and Brown 1979; Seifert et al. 1982). For the MD-derived compressibilities, little change with composition is observed, in contrast to results obtained by Kress et al. (1988).

The adiabatic compressibility is related to the isothermal compressibility by

$$\beta_S = \beta_T - \frac{TV\alpha_P^2}{C_P} \tag{4}$$

where C_P is the isobaric heat capacity per gram formula weight and α_P is the isobaric thermal expansivity. Kress et al. (1988) estimated the difference between β_T and β_S to be about 1%. Because of the much higher temperatures in the present set of simulation results, this difference approaches 3%. Acoustic velocity is related to the adiabatic compressibility by

$$V_P = \sqrt{(\rho\beta_S)^{-1}}. \tag{5}$$

The MD results yield a sound speed for albite melt of 3.2×10^3 m/s at 3000 K and 4 GPa; thus, an acoustic (density) wave travels across the MD cell in just under 1 ps. The results of Kress et al. (1988) extrapolate to a value of about 2.75×10^3 m/s for albite at 1500 K and room pressure and a density near 2325 kg/m^3.

Results obtained from this study demonstrate the potential of MD simulations to make reasonably accurate estimates of thermodynamic properties of network fluids. Heat capacities calculated and reported above extrapolate to values within about 0.25R of those for laboratory glasses, and estimates of expansivity and compressibility have been achieved to within a factor of four, when corrections are made using laboratory estimates of the pressure and temperature derivatives of these quantities. This suggests that simple pairwise-additive interaction potentials are useful for making preliminary estimates of properties, even in simulations of strongly bonded liquids with considerable covalent character. The great advantage of the MD method is that various parameterizations of potential energy can easily be tested and many compositions can be studied rapidly and at low cost in comparison with more precise but expensive laboratory studies.

TRANSPORT PROPERTIES

The dynamic property easiest to obtain from the results of MD simulations is the coefficient of self-diffusivity (D_i), which was obtained from mean-square particle displacements (MSD) for species i by means of the Einstein relation

$$D_i = \lim_{t\to\infty} \frac{\langle r_i^2 \rangle}{6t} \tag{6}$$

in which $\langle r_i^2 \rangle$ is the mean-square displacement of atoms of species i observed over time t. The self-diffusion coefficients for each ion were computed, and results are shown in Table 5 for all compositions and temperatures. In addition to determining the ionic self-diffusivities, we also computed the ionic conductivity of the melt, which is principally the result of the diffusive transport of Na. This calculation employs a technique independent of that used to determine Na self-diffusivity.

In the present study, we seek to delineate some of the constraints within which two-body, centro-symmetric potential energy functions are effective in estimating transport properties for multicomponent silicate melts. MD experiments with long-range interactions characteristic of silicate liquids have been of small size and brief duration because of the practical limitations in computing resources. Pioneering MD studies of silicates (including some on several compositions examined in the present study) presented MSD trajectories with durations of the order of 0.01 ns. As a result of the imposed time scale, these early studies explicitly regarded O diffusivity values of 10^{-6} cm^2/s as a boundary between "frozen" and "mobile" systems. For $D \approx 10^{-6}$ cm^2/s, the mean ionic displacement is about 0.8 Å in 0.01 ns. In the present study, we determined the diffusivities of all the ions over durations as long as 0.1 ns, for subsets of >70 to as many as 800 ions, depending on species, and assessed the reliability of the simulation results by comparison with laboratory measurements. In extending the ranges of system size and duration used in the simulations by as much as an order of magnitude, resolution of diffusivities smaller than those previously attempted (i.e., simulation at lower temperatures) becomes possible. The differences in diffusivity exhibited by Al, Si, and O in the melt may further serve to illuminate aspects of the mechanism of diffusion and viscous flow.

Na diffusivity and ionic conductivity

Representative results for Na mean-square displacement are presented in Figure 2, and diffusivities computed from Equation 6 are given in Table 5. In Table 6 the activation-energy results for Na are presented; values

TABLE 5. Ionic diffusivities (cm^2/s)

	2500	3000	3500	4000	4500
			N20		
Na	1.58×10^{-5}	2.40×10^{-5}	4.04×10^{-5}	6.04×10^{-5}	
Al	3.82×10^{-8}	1.96×10^{-7}	3.14×10^{-7}	3.19×10^{-7}	
Si	1.96×10^{-8}	1.03×10^{-7}	1.35×10^{-7}	2.01×10^{-7}	
O	2.82×10^{-8}	1.51×10^{-7}	2.05×10^{-7}	3.13×10^{-7}	
			N33		
Na	2.10×10^{-5}	3.00×10^{-5}	5.65×10^{-5}	5.58×10^{-5}	
Al	8.60×10^{-8}	1.70×10^{-7}	3.43×10^{-7}	4.80×10^{-7}	
Si	3.00×10^{-8}	6.52×10^{-8}	1.39×10^{-7}	1.57×10^{-7}	
O	4.67×10^{-8}	1.04×10^{-7}	2.87×10^{-7}	3.84×10^{-7}	
			N41		
Na	2.59×10^{-5}	3.39×10^{-5}	5.96×10^{-5}	8.28×10^{-5}	
Al	3.08×10^{-8}	1.15×10^{-7}	4.63×10^{-7}	5.02×10^{-7}	
Si	2.15×10^{-8}	6.99×10^{-8}	1.43×10^{-7}	1.38×10^{-7}	
O	2.30×10^{-8}	1.27×10^{-7}	3.24×10^{-7}	3.10×10^{-7}	
			N50		
Na	2.80×10^{-5}	5.20×10^{-5}	5.31×10^{-5}	1.15×10^{-4}	
Al	1.86×10^{-8}	2.07×10^{-7}	1.38×10^{-7}	3.61×10^{-7}	
Si	1.29×10^{-8}	1.23×10^{-7}	5.35×10^{-8}	2.09×10^{-7}	
O	1.52×10^{-8}	2.28×10^{-7}	1.06×10^{-7}	3.47×10^{-7}	
			N50*		
Na		3.96×10^{-5}			
Al		1.41×10^{-7}			
Si		7.18×10^{-8}			
O		1.37×10^{-7}			
			N60		
Na	3.42×10^{-5}	5.21×10^{-5}	6.86×10^{-5}	9.08×10^{-5}	
Al	7.08×10^{-8}	4.58×10^{-7}	3.25×10^{-7}	7.82×10^{-7}	
Si	4.06×10^{-8}	1.36×10^{-7}	1.54×10^{-7}	3.42×10^{-7}	
O	2.30×10^{-8}	1.27×10^{-7}	3.24×10^{-7}	3.10×10^{-7}	
			N60*		
Na			7.62×10^{-5}		
Al			3.91×10^{-7}		
Si			2.23×10^{-7}		
O			3.31×10^{-7}		
			N100		
Na	2.62×10^{-5}	6.39×10^{-5}	8.12×10^{-5}	1.06×10^{-4}	1.19×10^{-4}
Al	7.48×10^{-8}	1.71×10^{-7}	3.02×10^{-7}	1.54×10^{-6}	2.12×10^{-6}
Si	3.15×10^{-8}	1.21×10^{-7}	2.67×10^{-7}	1.04×10^{-6}	1.64×10^{-6}
O	7.21×10^{-8}	2.10×10^{-7}	3.82×10^{-7}	1.72×10^{-6}	2.38×10^{-6}
			N100*		
Na	2.47×10^{-5}	5.96×10^{-5}	7.70×10^{-5}		
Al	2.35×10^{-7}	3.24×10^{-7}	7.00×10^{-7}		
Si	1.90×10^{-7}	2.48×10^{-7}	4.52×10^{-7}		
O	2.45×10^{-7}	3.55×10^{-7}	7.48×10^{-7}		

* Compositions for which diffusivity results were obtained in replicate simulations.

of activation energy vary between 55 and 75 kJ/mol. Na self-diffusivity determined in the simulations is approximately 100 times that for O, and compositional variations of the activation energy are small and not systematic. However, the magnitude of diffusivity at each temperature does increase systematically with increasing content of $NaAlO_2$. This behavior is similar to that observed for Na diffusion in sodium silicate melts. For the series $Na_2O \cdot nSiO_2$ with n = 2, 3, 4, 5, 6, and 8 (10–35 mol% Na_2O), Johnson et al. (1951) report Na self-diffusivity in the temperature range 750–1250 K at 1 bar. We fitted these data and find them well represented by a relation of the form $D_{Na,self} = D_0 \exp(Ax)\exp(-E/RT)$ with $D_0 \approx 7 \times 10^{-7}$ m²/s, A = 10.9, and E = 92 kJ/mol. In this expression, x represents the mole fraction of Na_2O in the sodium silicate melt. The point here is that E is independent of composition, whereas the preexponential factor depends systematically on composition such that Na self-diffusion is faster in more sodic melts. This feature of the laboratory experiments of Johnson et al. (1951) is reflected in the results from the series of simulations presented here.

Na diffusivity was measured by Jambon and Carron (1976) in $NaAlSi_3O_8$ glass at temperatures from 623 to 1068 K and by Terai (1969) for $NaAlSiO_4$ glass in the range 473–873 K; the latter study also made measure-

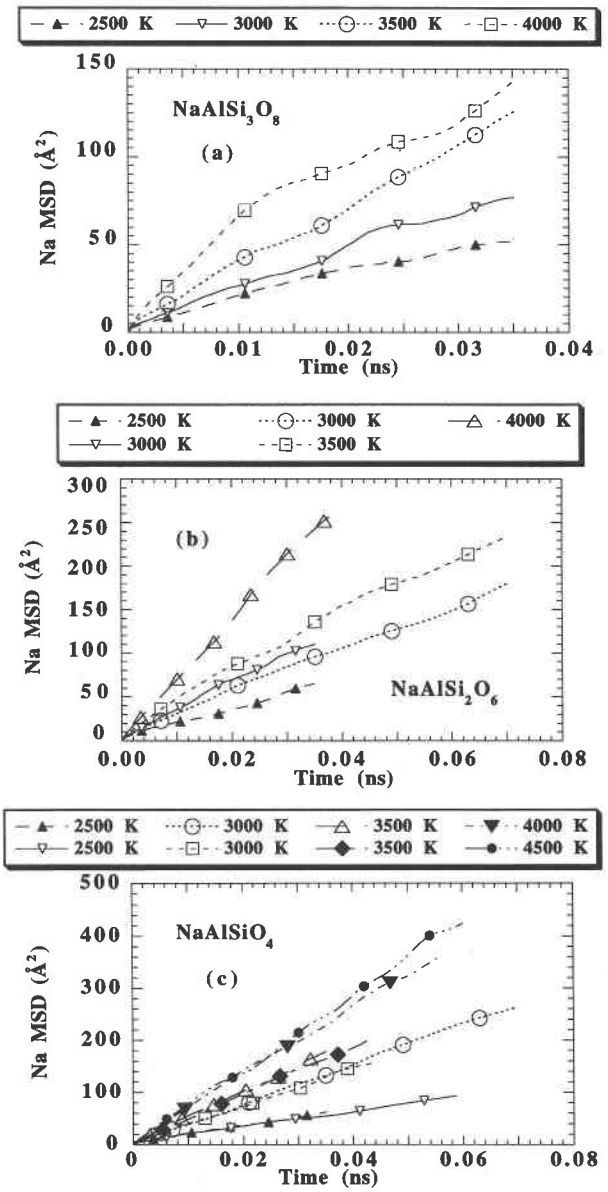

FIGURE 2. Na mean-square displacement at each experimental temperature for compositions $NaAlSi_3O_8$ (a), $NaAlSi_2O_6$ (b), and $NaAlSiO_4$ (c). Na diffusivity is approximately 100 times greater than diffusivities of Si, Al, and O. Isothermal diffusivity of Na increases with $NaAlSiO_4$ content; systematic compositional variations of activation energy for diffusion are not detectable. Results from replicate simulations indicated by separate symbols.

ments of ionic conductivity (see below). A study of Na diffusivity and electrical conductivity for an aluminosilicate composition very near that of N41 of the present study was made by Heckman et al. (1967). The activation energy for Na diffusion in $NaAlSi_3O_8$ (entirely below T_g) determined by Jambon and Carron was approximately 55 kJ/mol, and for $NaAlSiO_4$ the measurements of Terai gave 59.4 kJ/mol. Results published by Heckman et al.

TABLE 6. Arrhenius parameters for ionic self-diffusivities

	Log D_0	σ(Log D_0)	E_a	$\sigma(E_a)$
		Na		
N20	−3.274	0.129	−74.5	7.7
N33	−3.430	0.202	−60.1	12.0
N41	−3.248	0.178	−66.0	10.6
N50	−3.104	0.281	−70.9	16.6
N60	−3.330	0.052	−54.4	3.1
N100	−3.013	0.113	−73.3	6.8
		Al		
N20	−4.785	0.534	−120.5	31.7
N33	−5.035	0.093	−97.7	5.5
N41	−4.020	0.407	−166.0	24.2
N50	−4.509	0.787	−143.6	46.4
N60	−4.624	0.554	−115.4	33.6
N100	−4.294	0.440	−128.3	26.4
		Si		
N20	−4.983	0.449	−125.7	26.7
N33	−5.486	0.189	−97.0	11.3
N41	−5.321	0.367	−109.3	21.8
N50	−5.067	0.873	−126.1	51.5
N60	−5.032	0.264	−111.2	16.0
N100	−4.265	0.504	−140.0	30.2
		O		
N20	−4.735	0.437	−130.1	26.0
N33	−4.786	0.206	−122.6	12.3
N41	−4.362	0.532	−152.1	31.6
N50	−4.512	0.983	−145.7	58.0
N60	−4.243	0.461	−157.6	28.0
N100	−4.157	0.407	−133.9	24.4

Note: D_0 in squared centimeters per second; E_a in kilojoules per mole.

(1967) give a value of 63.1 kJ/mol. Figure 3 shows the MD results for Na diffusivity in relation to the lower temperature laboratory measurements of Jambon and Carron (1976), Terai (1969), and Heckman et al. (1967).

The MD observations of Na diffusivity (and particularly, its temperature variation) agree quite well when extrapolated to conditions for which experimental results are available. Calorimetric glass-transition temperatures for N33, N50, and N100 are given by Richet and Bottinga (1984) as 1096, 1130, and 1033 K, respectively. NMR studies of relaxation mechanisms related to Na diffusion (e.g., Stebbins et al. 1994) suggest that activation energy for Na diffusion in liquid silicates should vary little from that found in the experimental studies at temperatures not far below T_g. Detailed study of the population of O ions undergoing active site exchange (see below) reveals compositional variations in network mobility between $NaAlSi_3O_8$ or N41 and $NaAlSiO_4$. Despite these variations, and the requisite extrapolation in temperature, the activation energies observed in the MD experiments are consistent with the experimental results on glasses, although the intercepts of the diffusivity-temperature relation (D_0) are recovered less successfully.

Ionic conductivity determined in the simulations results almost entirely from the relatively rapid diffusion of Na. The conductivity $\sigma_{\alpha\beta}$ for ionic species α with respect to species β may be computed according to

$$\sigma_{\alpha\beta} = \frac{1}{3VkT}\int_0^\infty \langle \mathbf{J}_\alpha(t)\cdot\mathbf{J}_\beta(0)\rangle \, dt \qquad (7)$$

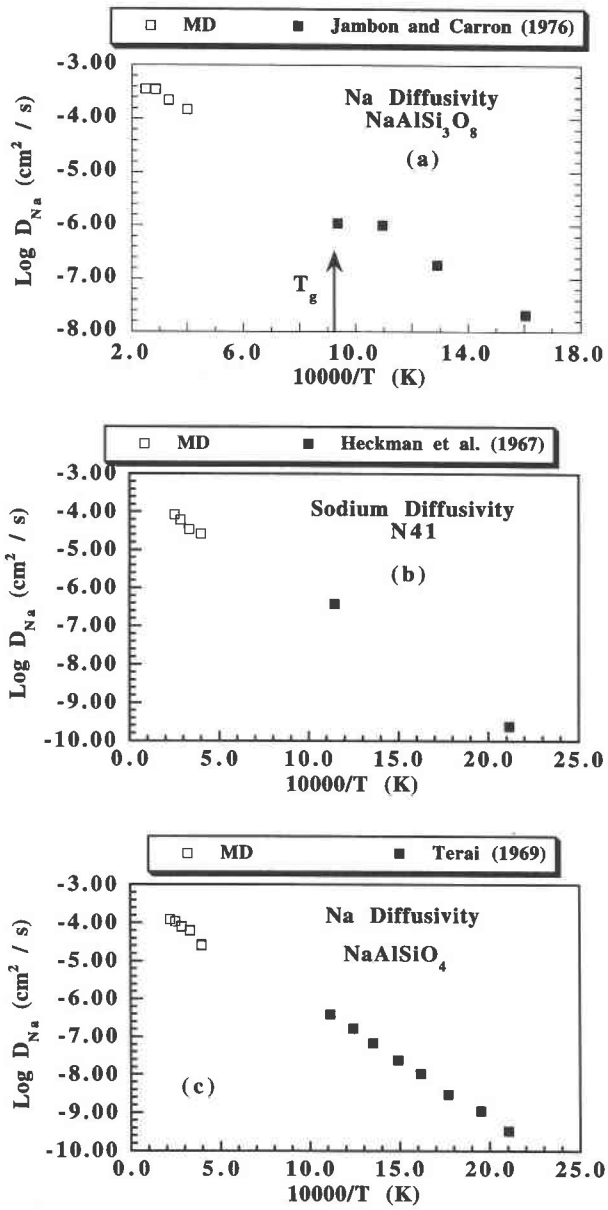

FIGURE 3. (a) Comparison of Na diffusivity for $NaAlSi_3O_8$ obtained in simulation (open squares) with that measured in laboratory (solid squares) by Jambon and Carron (1976). Temperature of glass transition measured by Richet and Bottinga (1984) is indicated by arrow marked "T_g". (b) Na diffusivity in simulation of N41 in comparison with that measured in almost the same composition by Heckman et al. (1967). Only upper and lower temperature limits of data of Heckman et al. (1967) are indicated. (c) Na diffusivity in simulation of $NaAlSiO_4$ in comparison with that measured by Terai (1969).

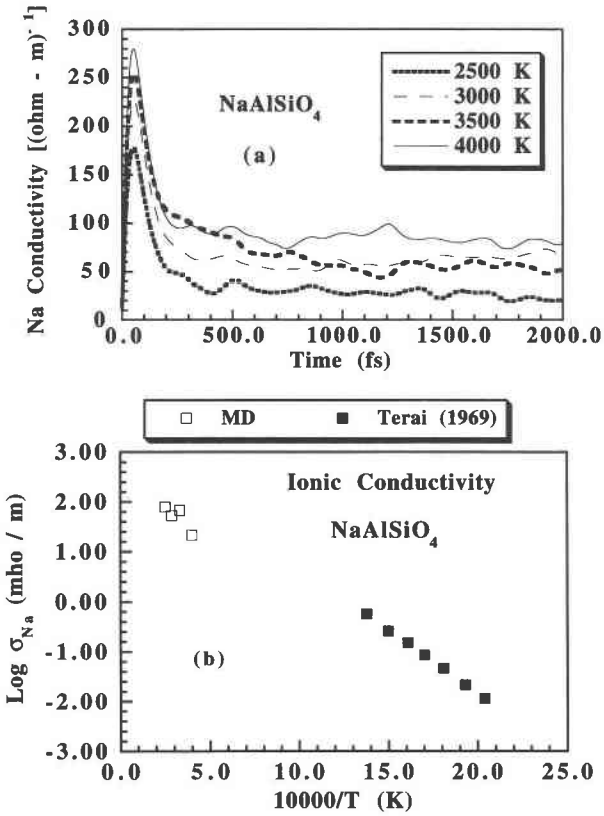

FIGURE 4. (a) Ionic conductivity due to Na in $NaAlSiO_4$ determined from simulations at four temperatures, calculated according to Equations 7 and 8 in text. (b) Ionic conductivity determined in simulations (open squares) in comparison with results of laboratory measurements by Terai (1969).

in which T is temperature, V is the system volume, and the bracketed expression in Equation 7 is the time average of the electric current correlation function during the simulation (Gillan 1991). $\mathbf{J}_z(t)$ represents the flux of charge in the system at time t,

$$\mathbf{J}_z = \sum_{\lambda} z_\lambda e \sum_{i=1}^{N_\lambda} \mathbf{v}_{\lambda i} \tag{8}$$

where the first sum is over all ionic species λ, the second sum is over all ions of species λ, and $\mathbf{v}_{\lambda i}$ is the vector of particle velocities for species λ at time t.

Ionic conductivity was computed by Equations 7 and 8 for $NaAlSiO_4$ at temperatures from 2500 to 4000 K. The integral (Eq. 7) for $\alpha = \beta =$ Na is plotted to 2 ps in Figure 4a. Figure 4b is an Arrhenius plot of the temperature variation of ionic conductivity in $NaAlSiO_4$. The resulting activation energy of 64 kJ/mol agrees fairly well with that determined by Terai (1969) for laboratory measurements of electrical conductivity, which gave a value of 49.3 kJ/mol for this composition, measured at significantly lower temperature, in the range 500–900 K.

O diffusivity and implications for viscous flow

Self-diffusion coefficients (D_i) of O, Si, and Al are presented in Table 5. To improve statistics for these more slowly diffusing ions, displacement trajectories were calculated on the basis of 50–200 distinct time origins each separated by 0.05–0.1 ps, and no sensitivity of the com-

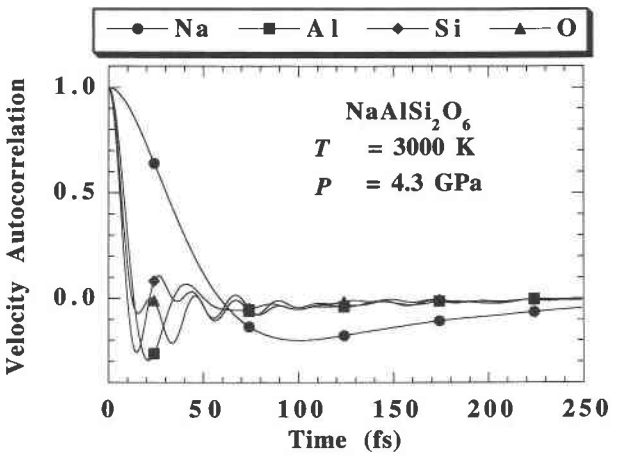

FIGURE 5. Velocity autocorrelation, $Z(t)$ (Eq. 9 in text), for each ion in $NaAlSi_2O_6$ at 3000 K. Calculation based on 1000 distinct time origins. Horizontal scale is time in femtoseconds.

puted diffusivity to the separation or number of time origins was detected. For the density and temperature of the simulations, the decay to the first minimum of the velocity-autocorrelation function (VAF), defined by

$$Z(t) = \frac{1}{N}\sum_{i=1}^{N}\frac{v_i(t)\cdot v_i(0)}{v_i(0)\cdot v_i(0)} \qquad (9)$$

for N particles of species i is typically about 10–25 fs for network-forming ions (Fig. 5). An alternate definition of D_i is given by integration of $Z(t)$, but as can be seen in Figure 5, small oscillations in $Z(t)$, which do not decay completely over the duration of the simulation, prevent accurate determination of D_i from the velocity autocorrelations. Hence, we chose to use the Einstein relation (Eq. 6) to compute D_i.

Figures 6a and 6b present graphically the MSD of O in all compositions at the extrema of temperature (4000 and 2500 K), and Figures 6c–6e display the MSD variation with temperature for the compositions $NaAlSi_3O_8$, $NaAlSi_2O_6$, and $NaAlSiO_4$, respectively. Each MSD curve represents a statistical sample of some 75000–80000 individual trajectories, each at least 0.04 ns in duration (i.e., typically computed from at least 100 distinct trajectory time origins for 750–800 O ions). The self-diffusion coefficients in Table 5 were obtained from Equation 6 by least-squares fits to the mean-square displacement results. Sampling error for D, estimated to be about 0.15 in logarithmic units, is based on results from replicate simulations performed for N50, N60, and N100 under ostensibly identical conditions but begun from different random starting configurations. For example, in Figure 6a, N100A and N100B refer to two such independent simulations. In Table 5, compositions for which diffusivity results were obtained in replicate simulations are indicated by asterisks. Additional matters pertaining to sampling error appear below in discussion of departures from ergodicity observed in the simulations.

In several previous MD simulations of silicates, 0.06 nm^2 was regarded as the minimum MSD for establishing reliable ionic diffusion rates. Resolution of diffusivities less than this arbitrary threshold ($D \approx 10^{-6}$ cm^2/s) is a function of adequate system size and simulation duration. Oscillatory behavior is apparent in some of the MSD trajectories, especially at lower temperatures, indicating effects of the motions of a few individual ions and the limits of meaningful averaging. O self-diffusivity for N20, N33, N41, N50, and N60 is $<10^{-6}$ cm^2/s, even at 4000 K (Table 5), and approaches this value at 3500 K only in N100. Below these temperatures, most O ions exhibit vibrational, but not diffusional motion on the time scale of these experiments; over the duration of the simulation (~40–70 ps), the RMS displacement does not exceed 0.25 nm. In the simulations, the temperature for this threshold of O diffusivity is above 4000 K for N33 and N50. Nevertheless, the O diffusivities determined in these simulations correspond to viscosities in the range of 0.001–0.1 Pa·s, estimated from the Stokes-Einstein and Eyring relations. These values are considerably higher than those predicted from Arrhenian extrapolation of lower temperature viscosity measurements, and this observation is discussed in detail below.

Because the trajectories were computed in the NVE ensemble (i.e., at constant density and total energy) the temperature variation of diffusivity is nonisobaric. Extreme pressure has been shown to increase the transport rates of network-forming species and decrease the diffusivity of the charge-balancing Na species (e.g., Angell et al. 1983). However, given estimates of activation volume from the laboratory and from concurrent MD experiments (Shimizu and Kushiro 1984; Bryce et al. 1994), the pressure variation from 2500 to 4500 K along the isochores (2–4 GPa) is not sufficient to influence significantly the variation of diffusivity with composition and temperature.

Results of linear regressions of log D vs. $1/T$ for the ions are compiled in Table 6. Figures 7a–7c show the Arrhenian variation of diffusivity of Na, Al, and Si for the representative compositions N33, N50, and N100, and Figure 7d shows the diffusivities of the network-forming ions in $NaAlSiO_4$. Figures 7e–7g present Arrhenius plots of O diffusivity for the same three compositions, additionally indicating diffusivities estimated in the range 1200–1500 K using the Stokes-Einstein (S-E) relation

$$D_i = \frac{k_B T}{6\pi\eta r_i} \qquad (10)$$

on the basis of extrapolations of laboratory viscosity measurements made at temperatures of 1100–1500 °C and at ambient pressure (Stein and Spera 1993). An S-E size parameter (r_i) value of 3.5 Å, the distance to the first minimum in $g_{O\text{-}O}(r)$, was used to estimate minimum values for equivalent O diffusivities from the viscosity measurements. It is important to note that the activation energy for O diffusion (Table 6) shows no systematic variation

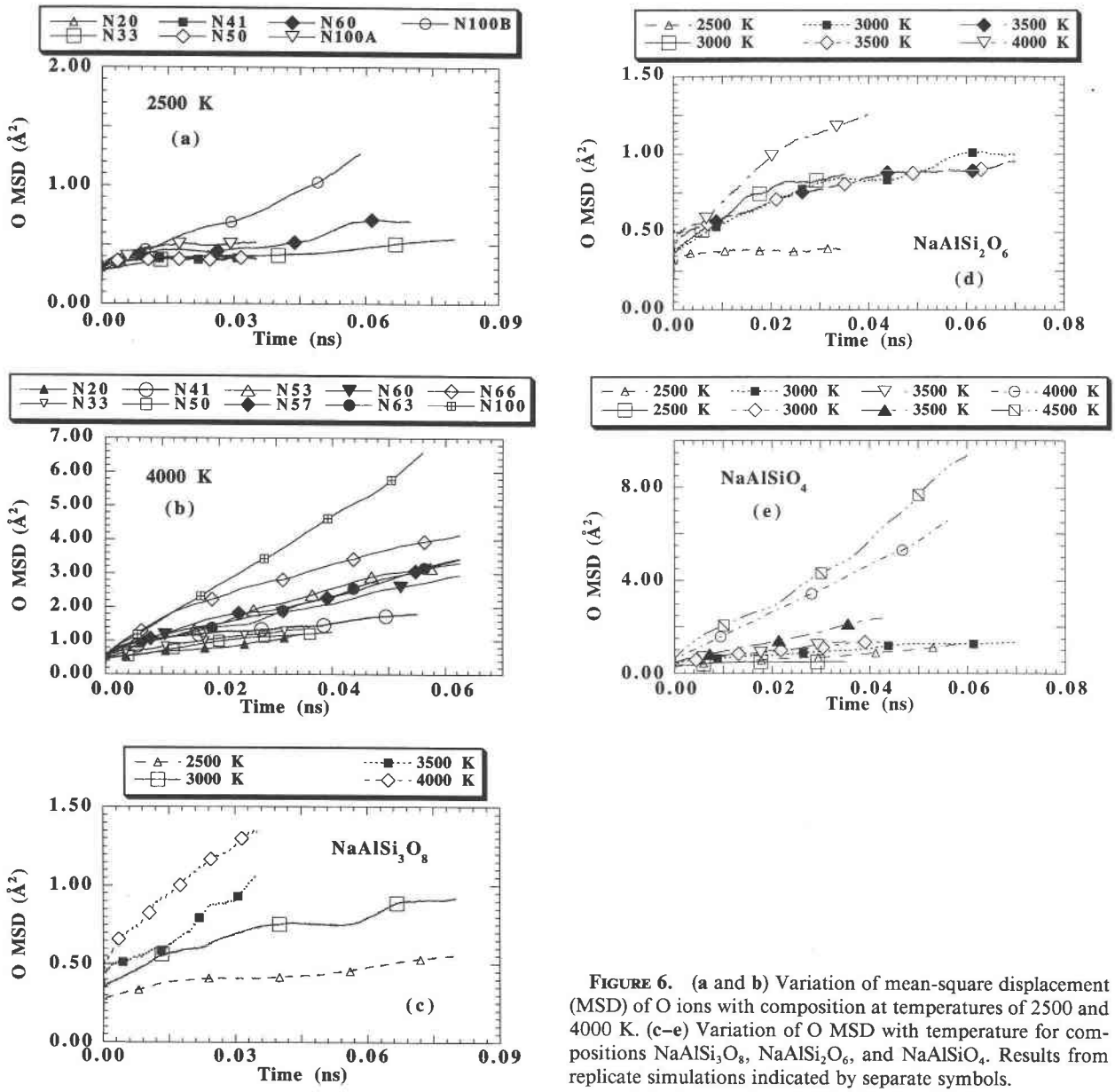

FIGURE 6. (a and b) Variation of mean-square displacement (MSD) of O ions with composition at temperatures of 2500 and 4000 K. (c–e) Variation of O MSD with temperature for compositions $NaAlSi_3O_8$, $NaAlSi_2O_6$, and $NaAlSiO_4$. Results from replicate simulations indicated by separate symbols.

with composition, with values generally near 140 ± 25 kJ/mol, and that the MD-generated activation energy is significantly lower than viscous activation energy measured for these compositions in the laboratory, which do in fact vary with composition. Specifically, a previous study (Stein and Spera 1993) found a linear relationship between E_η and composition, varying from about 340 kJ/mol for $NaAlSiO_4$ (N'Dala et al. 1984) to 470 kJ/mol for N20 [Urbain et al. (1982) reported 515 kJ/mol for SiO_2]. In Figure 7f we also plotted the O diffusivity measured experimentally by Shimizu and Kushiro (1984) for $NaAlSi_2O_6$ liquid at temperatures between 1673 and 1883 K and pressures of 0.5–2.0 GPa. The activation energy obtained by Shimizu and Kushiro (1984) is 280 kJ/mol at 1.5 GPa. Pressure in the N50 simulations remained between 2 and 4 GPa, somewhat higher than in the experiments of Shimizu and Kushiro. On the basis of the activation volume obtained by Shimizu and Kushiro (−6.3 cm^3/mol), the pressure increase to about 4 GPa in the simulations does not account for the reduced activation energy observed for O diffusion in the present series of MD computer experiments. The failure of the expected relationships between O diffusivity behavior in the simulations and viscosity measured in the laboratory suggests that, on the time scale of the MD experiment, a typical O ion does not participate in flow processes (see below).

The Eyring relation,

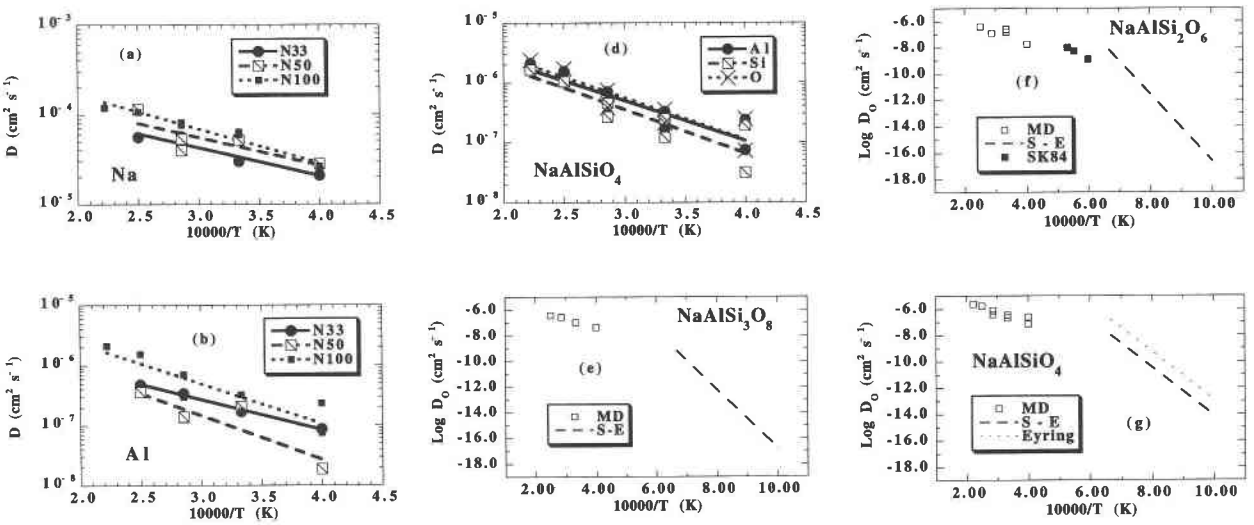

FIGURE 7. (a–c) Arrhenian variation of diffusivity with temperature for Na, Al, and Si, respectively, in the compositions N33, N50, and N100. Best-fit line is indicated in each case. (d) Arrhenian diffusivity of network-forming ions in $NaAlSiO_4$. Best-fit lines are indicated. (e–g) Comparison of O diffusivities in MD simulations with diffusivities estimated from Stokes-Einstein relation (Eq. 10) and viscosity results of Stein and Spera (1993). Open squares are O diffusivity results of simulations; bold dashed line is diffusivity computed from viscosity measurements in approximate temperature range of 1200–1600 K. In f, results of O diffusivity measurements by Shimizu and Kushiro (1984) are indicated by solid squares. In g, dotted line indicates diffusivities computed from measured viscosity by Eyring relation (Eq. 11).

$$D = kT/\lambda\eta \qquad (11)$$

was also used to estimate diffusivity from viscosity and vice versa. In this relation, λ refers to the distance of the diffusive jump, a distance that in this case is the O diameter. Because $6\pi r_O$ is an order of magnitude larger than λ, Equation 11 predicts a somewhat larger diffusivity (smaller viscosity) than Equation 10; Figure 7g illustrates this difference using the results of viscosity measurements in the range 1000–1500 K. When analyzed with Equations 10 and 11, the rates of O diffusivity observed in the simulations or in tracer diffusion experiments conflict with observed thermal and compositional variations of silicate melt viscosity and viscous activation energy. Experimental work by Oishi et al. (1975) and Yinnon and Cooper (1980) illustrates this inconsistency rather well. This observation suggests that the mobility of an O atom in a typical or predominantly structural or energetic state is not simply related to $d(\ln \eta)/d(1/T)$, the activation energy for viscous flow. Dunn (1982) found that laboratory results for O diffusion for melts in the system $CaMgSi_2O_6$-$CaAl_2Si_2O_8$ do not agree with predictions of the Eyring theory unless unrealistically large values of the ionic jump distances (λ) are assumed. The need to invoke a large value for λ seems to imply that a larger structural unit is needed to explain viscous flow. We find that the MD results support this idea (see below). In fact, as is demonstrated below, the activation energy for creation of the population of O sites in the excited state (anomalously coordinated and undergoing site exchange) closely mimics the viscous flow activation energy both in magnitude and apparent compositional dependence. This is perhaps the most important result of the present study and provides a crucial link between melt structure and transport properties, the search for which has become the focus of much current research in geomaterials (Navrotsky 1994).

CRITICAL TRANSITION IN RELAXATION PHENOMENA AT SHORT TIME SCALES

As is evident (Fig. 7), O diffusivity in the MD experiments fails to mimic patterns expected from viscosity measurements in this system. On average, O transport identified with the bulk diffusion coefficient is dominated by the population of O ions that remain confined to their structural cages on the time scale of the simulation (about 0.1 ns). Use of the self-diffusivity of O to estimate viscosity by means of the Stokes-Einstein or Eyring relations gives results that disagree by two to four orders of magnitude in the temperature range of the simulations. This divergence is unacceptable, even considering the large extrapolation from the extensive base of laboratory measurements at temperatures between 1000 and 1600 K [see Stein and Spera (1993) for a tabulation and review of these measurements]. Significantly, there is no observed compositional variation of the activation energy for O diffusion in the simulations. This implies that thermal perturbations of static structure (as related to the mech-

anisms of diffusion) in the MD model system are not significantly composition dependent (a small effect would be difficult to isolate unless much larger and longer numerical experiments were conducted). Suppression of such effects may result from intrinsic limitations of the two-body interactions used in the model or from the brief time scale of the simulations. In the following discussion, the latter interpretation is favored.

A persistent problem in molecular dynamics concerns the degree to which properties evaluated in the simulation approximate those of the liquid or of the glassy state of the material investigated (Hiwatari et al. 1994). To a considerable extent, this issue arises because of the short duration (typically a fraction of a nanosecond) available for observing the MD system. The small size of MD systems and the characteristically extreme quench rate make the careful consideration of this question even more important. Slowing the relaxation processes leads to an ergodicity-breaking transition that takes place in glass-forming systems on time scales characteristic of MD simulations (Barrat and Klein 1991; Wahnstrom 1991). The time scales are not characteristic of the phenomenological glass transition (commonly regarded to take place at a viscosity of 10^{12} Pa·s) but are instead characteristic of a much lower viscosity (1–1000 Pa·s) and overlap with the values currently accessible by high-performance computing. Recent computer experiments have successfully documented aspects of the transition, predicted by mode-coupling theory (MCT) (see Fredrickson 1988 for a review). The behavior is found to be quite general, observed in simulations of quite distinctive materials with diverse formulations of the interparticle interactions (molten salts: Signorini et al. 1990; metallic alloys: Lewis 1991; molecular liquids with hydrogen bonding: Sindzingre and Klein 1992). The current status of the theory itself and progress in its experimental testing are recounted by Kim and Mazenko (1992).

Mode-coupling theory

The fundamental assertion of MCT concerns the role of density fluctuations in the slowing down of relaxation behavior near the glass transition. The van Hove density-autocorrelation function (see below) is related directly to the probability distribution for individual particle displacements. A clear illustration of the onset of structural arrest is found in the time evolution of the van Hove function, especially as deviation occurs from the classical hydrodynamic treatment of material diffusion. The Fourier transform of the function into the reciprocal space domain is the self-intermediate scattering function, the time dependence of which resolves two slow relaxation processes, the slower being that of α relaxation and the faster, β relaxation. In what follows, analysis of the van Hove function is accompanied by observations of tagged particle dynamics in which the motion of specific particles is followed for long durations, and results indicate that a transition takes place in the mechanism of O diffusion at temperatures in the range 3500–4000 K. This transition displays a clear dependence on composition that, significantly, mimics variations of experimentally determined viscous flow activation energy (E_a) across the join $NaAlSiO_4$-Si_2O_4. The detailed dynamics are seen to contrast significantly with collective self-diffusivity obtained from O mean-square displacements. This change in diffusive mechanism occurs with increasing temperature and $NaAlSiO_4$ content, from one mechanism described by discrete hops between activated sites (jump diffusion) to one in which structure rearranges globally (free diffusion). For compositions of the highest silica content, at the lowest temperatures, the structure is very nearly frozen when viewed on the time scale of the experiments.

The van Hove density-autocorrelation function

As noted, the frequency of structural permutations is most effectively illustrated by single-particle properties rather than collective (or averaged) properties such as the self-diffusion coefficient. The spatial Fourier transform of the self-intermediate scattering function is known as the van Hove autocorrelation function

$$G_s(r, t) = \frac{1}{N} \sum_{i=1}^{N_\alpha} \langle \delta[r_i(t) - r_i(0) - r] \rangle \qquad (12)$$

for particles of species α. In Equation 12, the δ function counts the occurrences of particle displacements $r \pm \Delta r$ so that $G(r, t)$ provides information about the frequency of occurrence of any particle displacement r at time t with respect to some time origin. Note that $G(r, 0)$ is identical to the static pair-correlation function $g(r)$ familiar from, for example, X-ray diffraction experiments (see, e.g., Taylor and Brown 1979). The function

$$P(r, t) = 4\pi r^2 G_s(r, t) \qquad (13)$$

then gives the spatial probability at time t of finding a particle that has moved a distance r relative to its position at $t = 0$. Another form for $G(r, t)$ may be obtained by defining a particle-density function

$$\rho(r, t) = \sum_i \delta[r - r_i(t)]. \qquad (14)$$

In terms of $\rho(r, t)$, the van Hove function may be written as

$$G(r, t) = \frac{1}{N} \int \mathrm{d}r' \, \langle \rho[(r - r'), 0] \rho(r', t) \rangle \qquad (15)$$

which shows that $G(r, t)$ is related to the thermally excited density fluctuations within the glass or liquid. For sufficiently large r or t, pairs of ions are statistically independent so that $G(r, t)$ approaches ρ in the limit. Significantly, it is possible to show that if the liquid behaves as a macroscopic continuum, then $G(r, t)$ is directly related to the usual Fickian or hydrodynamic solution to the diffusion equation with constant D. That is, in the continuum limit,

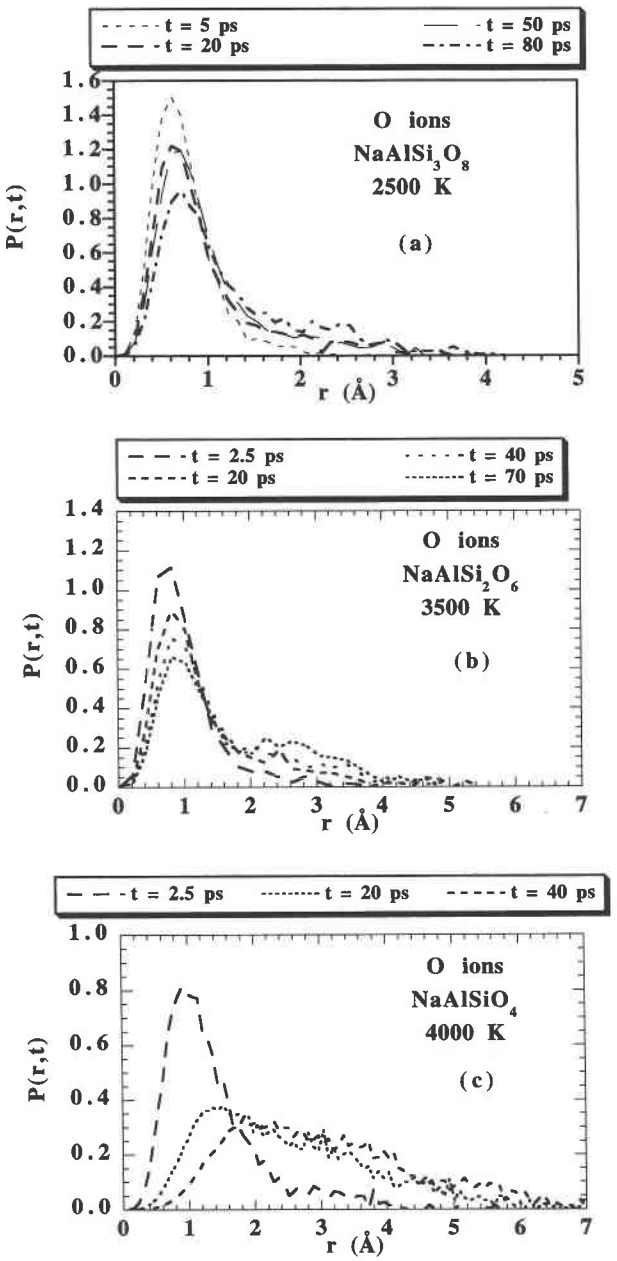

FIGURE 8. (a) $P(r, t)$ for O ions computed from van Hove density-autocorrelation function (see text). Figure shows results for $NaAlSi_3O_8$ at 2500 K. Peak of distribution shows little displacement even by 80 ps, although a small fraction of ions jumped a distance of 2.5 Å. (b) $P(r, t)$ for O in $NaAlSi_2O_6$ at 3500 K. Note decrease in mass of main peak with time and consequent growth of the small peak near the O-O nearest-neighbor distance, indicating diffusion by site-hopping mechanism. Location of main peak still shows very little displacement. (c) $P(r, t)$ for O in $NaAlSiO_4$ at 4000 K. Note significant decrease in amplitude, spatial displacement, and spreading out of main peak with time, indicating hydrodynamic behavior and the global rearrangement of silicate network rather than discrete jumps between O sites.

$$G_s(r, t) = \frac{1}{(4\pi Dt)^{3/2}} \exp\left(\frac{-r^2}{4Dt}\right). \tag{16}$$

Note that the mean-square value of r may be simply computed from Equation 16 according to

$$r^2 = \int_V r^2 G_s(r, t)\, dr = 6Dt \tag{17}$$

in agreement with the usual Einstein random-walk relationship presented earlier as Equation 6.

Patterns visible in the results for $P(r, t)$ clearly indicate that a transition occurs between glassy (frozen) and liquid behavior in the temporal, compositional, and temperature ranges of the simulations. Compositional influences in the time evolution of $P(r, t)$ are illustrated in Figure 8. The diffusion of O in $NaAlSi_3O_8$ at 2500 K is evidently frozen: the peak shows almost no movement in 80 ps (Fig. 8a). For $NaAlSi_2O_6$ at 3500 K (Fig. 8b), $P(r, t)$ shows the formation of a double peak at later times, indicating that diffusion occurred by jumps to nearest-neighbor sites in a still-frozen structure. The development of a second peak around 2–3 Å in Figure 8b is the earliest evidence of the breakdown of the continuum conceptualization. This is because of the jump-diffusion mechanism, dominated by T-O and O-O atomic interactions. By contrast, diffusion in $NaAlSiO_4$ at 4000 K (Fig. 8c) appears to take place by a gradual rearrangement of the entire structure in which no obvious clustering of particle displacements appears at the nearest-neighbor O-O distance. The computed pattern for $P(r, t)$ follows very closely the solution expressed in Equation 16 above. The contrasting temperature dependence of displacement of the peak (r_{max}) of $P(r, t)$ at increasing times for N41 and $NaAlSiO_4$ is shown in Figure 9. A transition from the site-hopping mechanism to spatially more-distributed structural rearrangement appears near 3250 K for molten $NaAlSiO_4$. This may be compared with the value for the peritectic composition (N60), which we estimate to be about 3500 K, and a value for $NaAlSi_2O_6$ of ~3800 K (Bryce et al. 1994). Studies of particle motion in simulations of simple liquids (Barrat et al. 1990; Barrat and Klein 1991, and incorporated references) indicate that decreasing temperature or increasing density (i.e., increasing pressure) induces the same qualitative effect on this transition from ergodic to nonergodic behavior in particle displacements.

By analysis of successive temporal displacements of r^*_{max} (the distance to the first maximum of the van Hove correlation function; see Fig. 9) it is possible to make a crude estimate of the critical mode-coupling temperature (T_c). This temperature corresponds to the transition from ergodic to nonergodic sampling of phase space during the time interval of the computer experiment. From a mechanistic point of view, this transition corresponds to a change from cooperative (global) structural rearrangement at $T > T_c$ to site hopping at $T < T_c$. The latter case closely resembles solid-state diffusion, whereas in the former, the hydrodynamic solution given by Equation 17 is valid within the duration of the MD experiment. It is

important to note that this transition occurs at temperatures that are much higher (with correspondingly lower viscosities) than those that characterize the calorimetric glass transition (T_g). The validity of this distinction is not altered by the vastly greater cooling rates typical of MD experiments in comparison with even the fastest laboratory quench techniques (e.g., melt spinning), which can elevate T_g by several hundred degrees [see Scherer (1986) for a discussion on estimating T_g from the cooling rate $|q|$].

In a companion study, Bryce et al. (1994) recovered accurate values of activation energy and activation volume for O diffusivity in $NaAlSi_2O_6$ in simulations that demonstrated ergodicity at temperatures of 4000–5000 K and at pressures up to 30 GPa. In this case, the majority of the O ions are mobile during the simulation, and thus the sampling time and system size result in an average (MSD), which correctly corresponds to temperature and pressure variations of diffusive behavior measured in the laboratory. Intercepts for the Arrhenius relation (D_0 values) agree less closely and remain a function of the parameterization of the interatomic potential. Use of different values of A_{ij} and B_{ij} in the Born-Mayer repulsion terms enables one to obtain higher D_0 values without significant changes in E_a [e.g., see results for $NaAlSi_3O_8$ of Scamehorn and Angell (1991)].

O-site exchange observations and mechanism of viscous flow

From the inception of the MD technique, its application in illustrating diffusive mechanisms has focused on the cooperative nature of the particle displacements (e.g., Woodcock et al. 1976; Kubicki and Lasaga 1988) and the anomalous coordination structures associated with particles actively undergoing site exchange (Brawer 1985). Observation of diffusive events in the two extreme mass-transport regimes noted earlier in the discussion of the van Hove function reveals that they are dominated by interactions among only the most mobile particles in the simulations. In the final section of this paper, we show that site exchange within this population of anomalously mobile O ions constitutes a thermally activated process with an apparent Arrhenian E_a, which agrees well with that measured for viscous flow in the laboratory and which also shows a significant (and consistent) variation with composition. In contrast, as noted earlier, estimates from bulk self-diffusivity using the Stokes-Einstein or Eyring relations differ by as much as a factor of 1000. Similarly, computed E_a for bulk O self-diffusion determined in the simulations (Table 6) does not vary significantly with composition, in contrast with laboratory results cited earlier.

Depending on composition and temperature, motions of 50–99% of network-forming ions involve only oscillations within potential wells formed by their near neighbors during the simulation. The pattern of O-site exchange is here described through the use of tagged particle dynamics, and results confirm that diffusive events al-

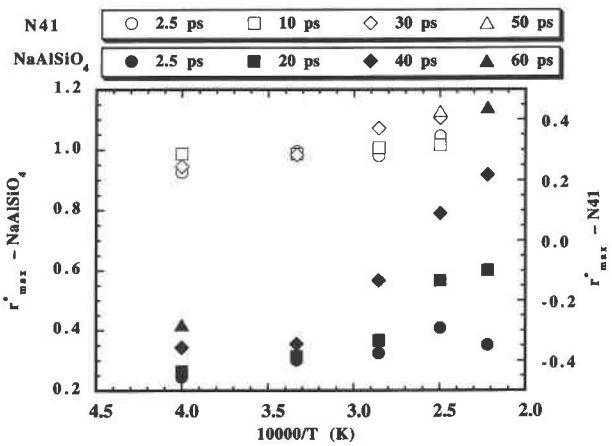

FIGURE 9. Time variation of location of peak of $P(r, t)$ for O ions in N41 and $NaAlSiO_4$ at the various simulation temperatures. Note that temperature for initiation of peak displacement for N41 is above simulation temperatures. Vertical axis is location of $P(r, t)$ peak scaled by most-probable O-O distance determined from pair-correlation function.

most invariably involve several anomalously mobile particles that become near neighbors during the site-exchange process. The high degree of correlation in the motions of the diffusing O ions observed in the simulations provides additional insight into the mechanism of viscous flow in network silicates. Most significant, the rate of site exchanges involving these particles yields a relaxation time that agrees with that extrapolated from lower temperature laboratory viscosity measurements to within an order of magnitude, and for some compositions within a factor of two. Additionally, a compositional dependence quite similar to that of the activation energy for viscous flow is recovered.

The quantity sought is the frequency of O near-neighbor interactions that result in atomic displacements greater than some threshold value. The rules for finding this quantity were as follows. First, the set of anomalously mobile O ions was determined such that a selected ion attained a minimum displacement relative to its time origin of 3 Å, clearly placing that ion outside its original potential well either by a mechanism of site exchange (hopping) or by cooperative motion of its set of neighbors. The distance criterion was chosen to be slightly greater than the most probable O-O separation determined from the O-O pair-correlation function $g(r)$ [defined in Stein and Spera (1995) and in incorporated references]. In the situation depicted in Figures 8a and 8b, this process occurs by site exchange. As shown in Figure 8c, occurrences of several site exchanges simultaneously in various parts of the system lead to reorganization of the framework as a whole and the breakdown of the reference frame for sites undergoing exchange.

The second step of the procedure was to note the time step during the simulation at which pairs from the list of mobile or anomalous O ions became near neighbors. In

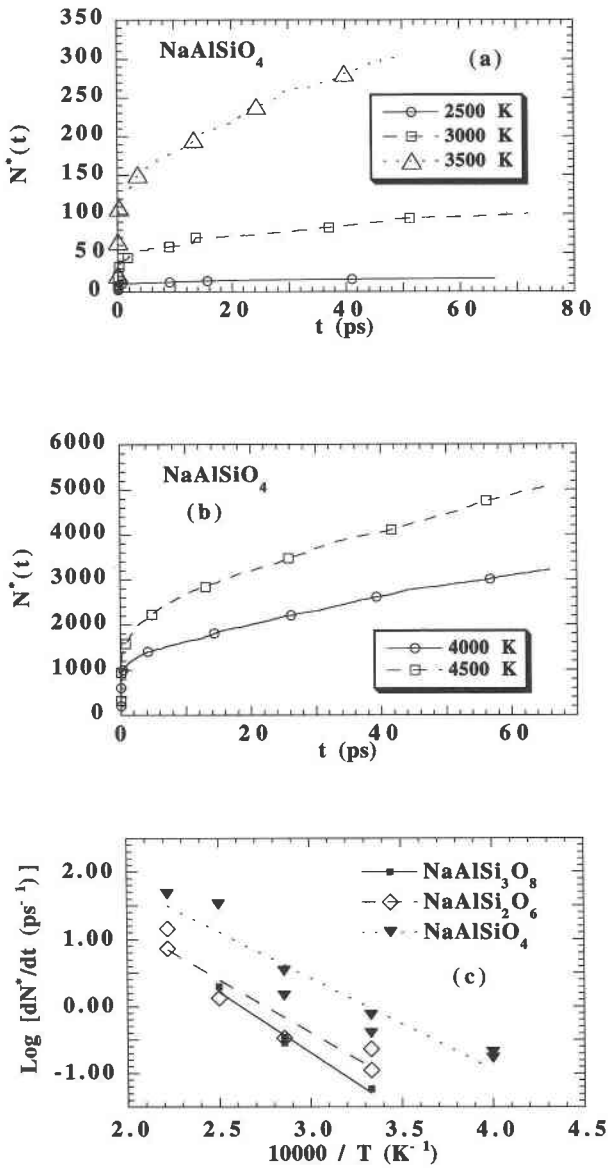

FIGURE 10. (**a** and **b**) Variation with time of number (N^*) of O-O site-exchange interactions within mobile ion population at indicated temperatures in $NaAlSiO_4$. (**c**) Arrhenius plot of limiting rate of increase of N^* with time for indicated compositions. Apparent Arrhenian activation energies associated with these rates are 260 kJ/mol for $NaAlSiO_4$, 310 kJ/mol for N60 (peritectic composition), 300 kJ/mol for $NaAlSi_2O_6$, and 350 kJ/mol for $NaAlSi_3O_8$.

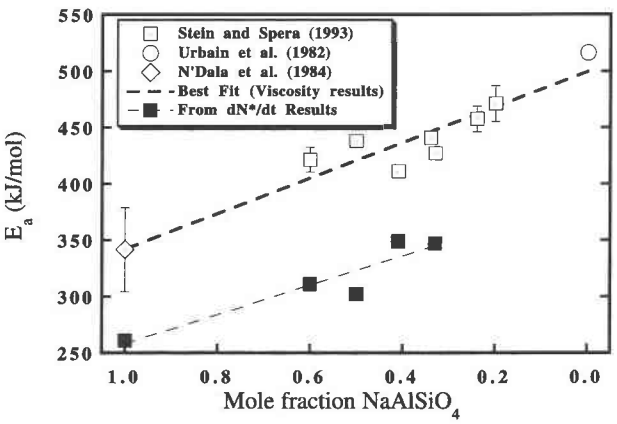

FIGURE 11. Compositional variation of apparent activation energy of dN^*/dt in comparison with that of activation energy measured for viscous flow.

most cases, anomalous O ions became neighbors only after occurrences of site exchange or other diffusive translations, although some of these pairs began the simulation as neighbors. This step is based on the hypothesis that the mechanisms responsible for O transport depend dominantly on cooperative motion and that isolated diffusive motion of a single ion almost never occurs (e.g., by a mechanism involving vacancies). In short, members admitted to the list were specific O ions involved in site exchange with their neighbors. Neighbor-pairs were selected regardless of whether significant motion of one or both atoms had occurred at the time, and each unique pair was listed along with the time step of the simulation at which the encounter originated; resolution of this time was limited to 0.05 ps precision.

A plot of the time variation of the cumulative number (N^*) of these interactions for $NaAlSiO_4$ is shown in Figure 10. The initial rise in N^* is due to the population of (eventually) mobile O ions that happened to be near neighbors at the start of the simulation. Following this transient, the relation attains a limiting slope that defines a characteristic time (rate of formation of new pairs, or exchange frequency). The magnitude of this limiting slope is composition dependent, and its temperature variation is described by the Arrhenius relation, as shown for the compositions $NaAlSi_3O_8$, $NaAlSi_2O_6$, and $NaAlSiO_4$ in Figure 10c. As shown in Figure 11, the apparent activation energy (E_N^*) for this relation varies from 350 kJ/mol for $NaAlSi_3O_8$ to 310 kJ/mol for N60, 300 kJ/mol for $NaAlSi_2O_6$ (N50), and 260 kJ/mol for $NaAlSiO_4$. These activation energies are in fair agreement with those for viscous flow measured in the experiments of Stein and Spera (1993). In particular, the variation of this apparent activation energy with composition appears to be quite similar to that measured for viscous flow in the range 1000–1500 K. There is a decrease of about 150 kJ/mol for the activation energy of O-site exchange (and hence, viscosity) for the coupled substitution reaction Na + Al $\rightleftharpoons$ Si across the join $NaAlSiO_4$-SiO_2. The differences in the magnitude of E_N^*, which approach 100 kJ/mol at each composition, may be related to the choice of particular potential interaction parameters. A longer discussion of this may be found in Stein and Spera (1995).

Finally, we note that there appears to be a compensation effect between the temperature dependence of dN^*/dt and the critical temperature of nonergodic behavior. Compositions rich in $NaAlSiO_4$ with $T_c \approx 3300$ K (at 2–3 GPa) are characterized by values of $\partial[\ln(dN^*/dt)]/\partial(1/$

T) (i.e., E_N*) near 250 kJ/mol, whereas for molten $NaAlSi_3O_8$ (N33), $T_c > 4000$ K and E_N* is ~350 kJ/mol. To study the quality of this compensation correlation, additional simulations of especially long duration are needed.

The limiting value of dN^*/dt defines a time constant (or frequency) that may be used to estimate a viscosity appropriate to the observed rate of O transport. The unrelaxed shear modulus for sodium aluminosilicates in this range of composition is ~30 GPa (Bansal and Doremus 1986). Figure 12 translates the rates represented by the slopes shown in Figure 10 to representative values for viscosity determined from the shear modulus and shows estimates derived from the extrapolation of the Arrhenian relationships for viscosity of $NaAlSi_3O_8$, $NaAlSi_2O_6$, and $NaAlSiO_4$ quoted from the experimental results of Stein and Spera (1993). Two related time constants for O diffusivity may be identified directly by examining the displacements of individual particles shown in Figure 13 for O in $NaAlSi_3O_8$ at 3000 K, which is well below the critical temperature of the ergodic to nonergodic transition of roughly 4250 K. The first is the duration of site-exchange motion, typically about 0.5 ps, and the second is the time between jumps, estimated here to be between 20 and 40 ps but which varies with temperature and composition, just as the viscosity of melts in this system varies with temperature and composition. This latter quantity is closely related to the value of $(dN^*/dt)^{-1}$ and gives an alternative statistical description of O transport at temperatures well below T_c, but typical durations and numbers of particles in the present series of simulations are not entirely adequate for this purpose.

The cooperative aspects of O transport are more easily observed in hopping systems such as that depicted in Figure 8b. One manifestation of this type of correlated jump motion is the oscillatory behavior of the mean-square particle displacements frequently observed at lower temperatures (see Fig. 6). In more mobile systems, these interactions are so numerous that the list of mobile O ions extends through the entire simulation-cell volume. Detailed examination of the trajectories of the most mobile ions illustrates the above concepts more concretely. Figure 14 shows examples of the spatial trajectories of atoms projected onto the x-y plane, shown for $NaAlSiO_4$ at 4500 K. For Na (Fig. 14a), the trajectory appears as a through-going motion punctuated by restrictions to volumes 2–6 Å in their largest dimension. This type of motion is observed regardless of temperature or composition. For O (Fig. 14b), the diffusive motion consists of vibrations within a slowly deforming cage of neighbors, the membership of which gradually changes; for less mobile compositions and temperatures, the motion is restricted to smaller volumes (areas). This atom-scale feature is consistent with more systemwide aspects of O diffusion. The hopping behavior seen for O in $P(r, t)$ in Figure 8b is the result of O motion within restricted spatial and temporal regions (cages). This can also be seen in the VAF (Fig. 5), in which short-time backscattering indicates the level of confinement for the network-forming species. In Figure 8c, virtually all O sites become involved in a mobilized region during some period of the simulation, and a reference frame in which activated sites may be identified

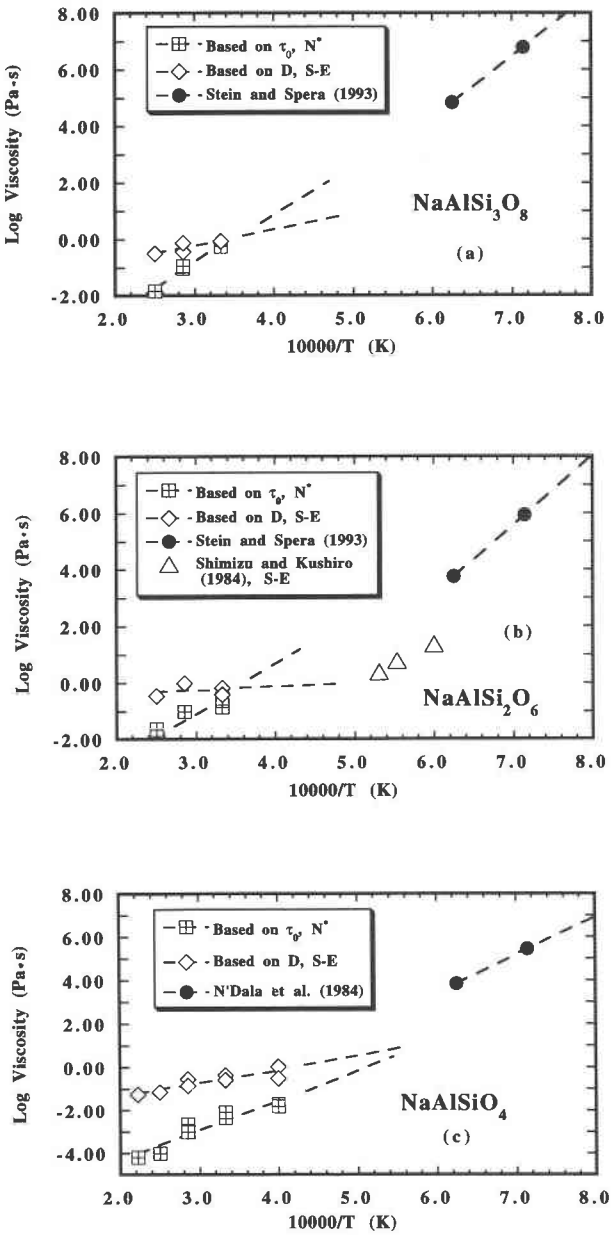

FIGURE 12. Comparison of measured viscosity and results from analysis of tagged particle dynamics for O ions in $NaAlSi_3O_8$ (**a**), $NaAlSi_2O_6$ (**b**), and $NaAlSiO_4$ (**c**). Open squares with crosses indicate viscosity computed from τ_0 obtained with $N^*(t)$ relation and infinite-frequency shear modulus. Circles = measured viscosities from indicated sources, and diamonds = simulation results for bulk O self-diffusivity, converted to viscosity by Equation 10. In **b**, triangles are viscosities computed from diffusivity measurements of Shimizu and Kushiro (1984) using Equation 10.

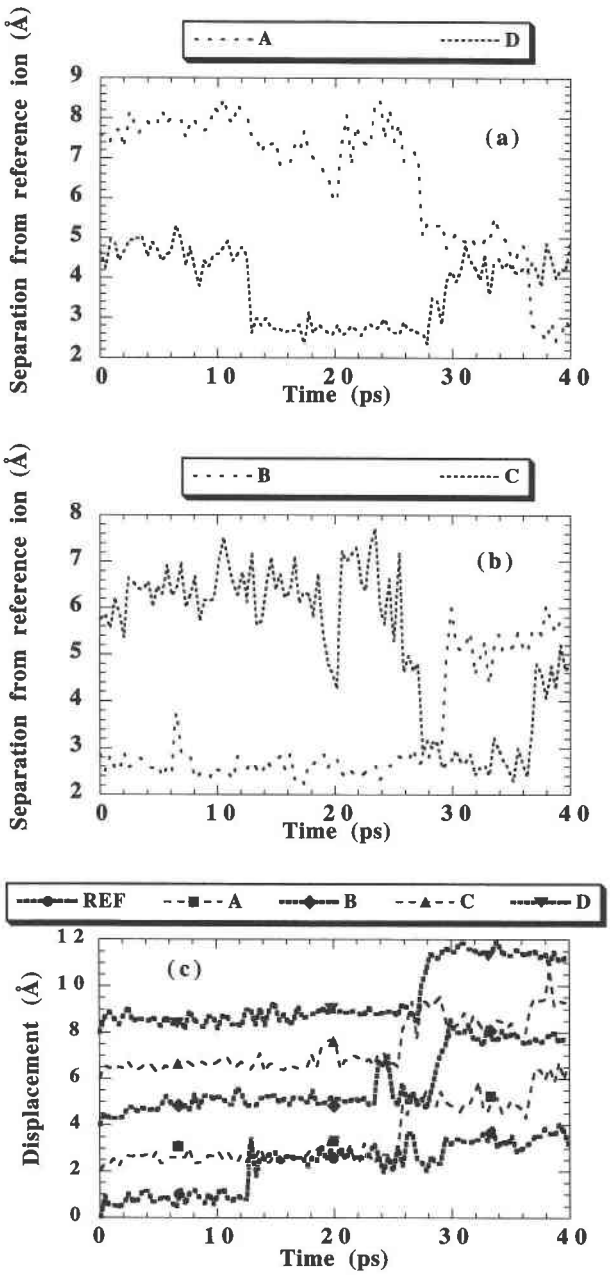

FIGURE 13. (a and b) Separations of four O ions from a reference ion, each of which eventually becomes a near neighbor of the reference ion during the simulation. Composition is $NaAlSi_3O_8$ at 3000 K. Diffusion mechanism is by discrete site exchange in a rigid framework. (See text discussion accompanying Fig. 8.) Note correlations of jumps by atoms B and C with a jump by A at about 28 ps, and by atom A with a jump by C at about 36 ps. Large excursions by C and A, which do not lead to site exchange, occur at about 20 ps. (c) Secular displacements with respect to time origins of each of the ions in a, including that of the reference ion, REF. Spatial origins for each ion are offset, and displacements are presented only with respect to the time origin. A burst of site-exchange activity at around 26–30 ps is evident.

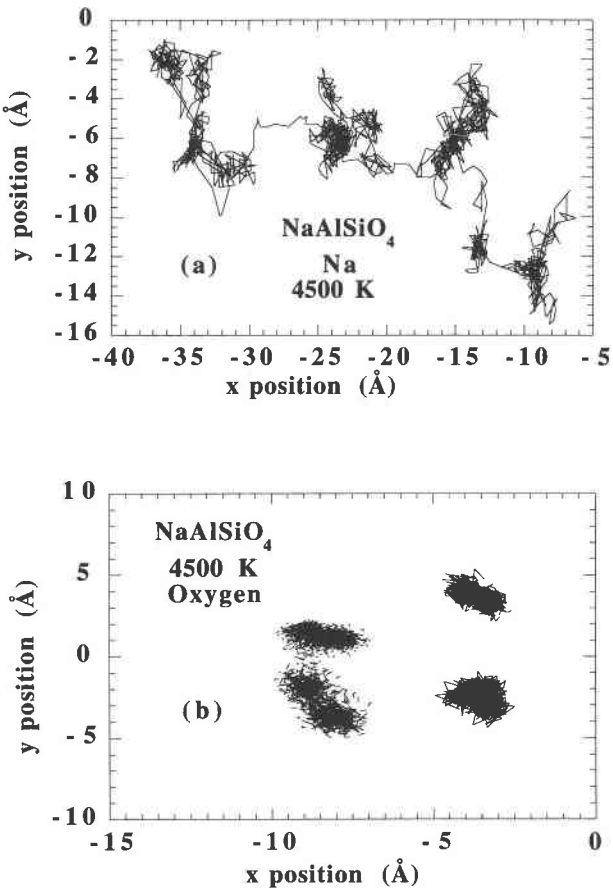

FIGURE 14. (a) Trajectories of several Na ions in $NaAlSiO_4$ at 4500 K projected onto x-y plane. Diffusion is by a through-going mechanism along structural channels, punctuated by more restricted motions in regions about 5 Å in linear dimension. Trajectories of ions were unfolded, reversing the application of periodic boundary conditions. (b) Trajectories of O ions projected onto x-y plane; simulation of $NaAlSiO_4$ at 4500 K. Note that motion takes place within restricted (but evidently spreading) regions larger than O-O nearest-neighbor coordination volumes.

is no longer available; in Figure 14b this appears as a gradual delocalization of the volumes of O cages.

CONCLUDING REMARKS

The present study demonstrates that molecular dynamics simulations using simple pairwise-additive potential energy functions are capable of making preliminary or reconnaissance estimates of material properties, including their temperature and composition derivatives, for molten silicates under conditions that are difficult, time consuming, and expensive to attain in the laboratory. For the sodium aluminosilicates, heat-capacity values were recovered to within 0.25R, expansivity and compressibility to within a factor of two to four, and activation energy for Na diffusion and ionic conductivity to within 15%. Diffusion of the network-forming ions Al, Si, and

O was theoretically related to viscous flow in these compositions, but in the MD experiments, the slope (activation energy) and intercept (D_0) results for the Arrhenius relation diverge from those expected from analysis of viscometric data for the same compositions.

The experimental time scales achievable with high-performance computational techniques were used here to explore the transition between ergodic and nonergodic thermodynamic states of the MD system. Below the temperature of this critical transition, T_c, the bulk diffusive behavior of network formers reflects the dominantly immobile condition of the ions. However, for the small fraction of ions that are mobile during the MD experiment, the dynamics of site exchange proceeds at time scales that much more closely match those expected for viscous flow at the experimental temperatures. In addition, activation energy for the site-exchange process agrees to within about 20% and displays a compositional variation quite similar to that observed for viscous flow at lower temperatures.

The calorimetric glass transition is important in experimental studies of relaxation mechanisms in silicates, but molecular dynamics experiments are not presently capable of accessing time scales relevant to this thermal state. Simulation experiments on silicates involve extrapolations of thousands of degrees from the range of MD temperatures to that of laboratory measurements and require quench rates $>10^{13}$ K/s. However, the present study provides evidence that relaxation times and mechanisms in molten silicates can be recognized through the use of density-correlation functions, particularly the van Hove density autocorrelation, and detailed examination of atomic motions by tagged particle dynamics. Transport properties determined by time-correlation functions reveal patterns that can be related to particular time scales. For the low-temperature states, time averaging becomes ineffective in sampling the relevant phase space, particularly for the small systems that are used in simulation studies. The ergodic assumption that ensemble averages are equivalent to time averages becomes invalid when the relaxation times of the system are longer than experimental time scales. However, some relaxation time scales detected in the results of the present study do meet this criterion and approximate those tentatively identified with mechanisms of viscous flow.

The model of silicate melt behavior utilized in these simulations is dominated by differences in the potential energy functions for the Si-O bond and for the longer and weaker Al-O bond. Compositional variation in our simulations is restricted to charge-balancing replacement of Si^{4+} in the network with $Al^{3+} + Na^{+}$. The result is an increase (at constant temperature) in the diffusivity of O and a decrease in the critical temperature of the ergodic to nonergodic transition with the increasing substitution of Al in the network (hence, introduction of smaller intertetrahedral bridging angles and higher average coordination number for Al and Si). The observed behavior of these simulated systems accords with Brawer's (1985) notion that different regions of the viscous liquid possess varying characteristic levels of thermal excitation. The rate of relaxation of these regions, according to Brawer, is related to the original level of excitation (and possibly to the size of the region).

Acknowledgments

This research was conducted with financial support from the U.S. Department of Energy (DE-FG03-91ER14211) and the National Science Foundation [EAR-9303906 (Geochemistry)]. The authors express appreciation to J.R. Rustad, D.A. Yuen, and J.G. Bryce for assistance and advice. Thoughtful reviews by Jim Rustad and one anonymous reviewer improved the presentation. Computational resources were provided by NASA Ames Research Center, the San Diego Supercomputer Center, and the National Energy Research Supercomputer Center at Lawrence Livermore National Laboratory. This is contribution 0196-35CM of the Institute for Crustal Studies, University of California, Santa Barbara.

References cited

Allen, M.P., and Tildesley, D.J. (1987) Computer simulation of liquids, 385 p. Oxford University Press, New York.

Angell, C.A. (1988) Perspective on the glass transition. Journal of the Physics and Chemistry of Solids, 49, 863–871.

——— (1991) Relaxation in liquids, polymers and plastic crystals: Strong/fragile patterns and problems. Journal of Non-Crystalline Solids, 131–133, 13–31.

Angell, C.A., Cheeseman, P., and Tamaddon, S. (1983) Water-like transport property anomalies in liquid silicates investigated at high T and P by computer simulation techniques. Bulletin de Minéralogie, 106, 87–97.

Bansal, N.P., and Doremus, R.H. (1986) Handbook of glass properties, 680 p. Academic, San Diego, California.

Barrat, J.-L., Roux, J.-N., and Hansen, J.-P. (1990) Diffusion, viscosity and structural slowing down in soft sphere alloys near the kinetic glass transition. Chemical Physics, 149, 197–208.

Barrat, J.-L., and Klein, M.L. (1991) Molecular dynamics simulations of supercooled liquids near the glass transition. Annual Reviews of Physical Chemistry, 42, 23–53.

Bengtzelius, U., Götze, W., and Sjölander, A. (1984) Dynamics of supercooled liquids and the glass transition. Journal of Physics C: Solid State Physics, 17, 5915–5934.

Berendsen, H.J.C., Postma, J.P.M., van Gunsteren, W.F., DiNola, A., and Haak, J.R. (1984) Molecular dynamics with coupling to an external bath. Journal of Chemical Physics, 81, 3684–3690.

Brawer, S. (1981) Defects and fluorine diffusion in sodium fluoroberyllate glass: A molecular dynamics study. Journal of Chemical Physics, 75, 3510–3521.

——— (1985) Relaxation in viscous liquids and glasses, 220 p. American Ceramic Society, Columbus, Ohio.

Bryce, J.G., Spera, F.J., and Stein, D.J. (1994) Accurate evaluation of P,T dependence of oxygen self-diffusion in molten $NaAlSi_2O_6$ by molecular dynamics (MD). Eos, 75, 713.

Dunn, T. (1982) Oxygen diffusion in three silicate melts along the join diopside-anorthite. Geochimica et Cosmochimica Acta, 46, 2293–2299.

Farnan, I., and Stebbins, J.F. (1990) Observations of slow atomic motions close to the glass transition using 2-D ^{29}Si NMR. Journal of Non-Crystalline Solids, 124, 207–215.

——— (1994) The nature of the glass transition in a silica-rich oxide melt. Science, 265, 1206–1209.

Fredrickson, G.H. (1988) Recent developments in dynamical theories of the liquid-glass transition. Annual Review of Physical Chemistry, 39, 149–180.

Gillan, M.J. (1991) The molecular dynamics calculation of transport coefficients. Physica Scripta, T39, 362–366.

Goldstein, M. (1969) Viscous liquids and the glass transition: A potential energy barrier picture. Journal of Chemical Physics, 51, 3728–3739.

Haile, J.M. (1992) Molecular dynamics simulation: Elementary methods, 489 p. Wiley, New York.

Hansen, J.P., and McDonald, I.R. (1986) Theory of simple liquids, 556 p. Academic, New York.

Heckman, R.W., Ringlien, J.A., and Williams, E.L. (1967) Sodium diffusion and electrical conductivity in sodium-aluminosilicate and sodium-calcium-aluminosilicate glasses. Physics and Chemistry of Glasses, 8, 145–150.

Hiwatari, Y., Matsui, J., Uehara, K., Muranaka, T., Miyagawa, H., Takasu, M., and Odagaki, T. (1994) Study of the α and β relaxations in a supercooled fluid via molecular-dynamics simulations. Physica A, 204, 306–327.

Jambon, A., and Carron, J.-P. (1976) Diffusion of Na, K, Rb, and Cs in glasses of albite and orthoclase composition. Geochimica et Cosmochimica Acta, 40, 897–903.

Johnson, J.R., Bristow, R.H., and Blau, H.H. (1951) Diffusion of ions in some simple glasses. Journal of the American Ceramic Society, 34, 165–172.

Kalen, J.D., Boyce, R.S., and Cawley, J.D. (1991) Oxygen tracer diffusion in vitreous silica. Journal of the American Ceramic Society, 74, 203–209.

Kim, B., and Mazenko, G.F. (1992) Mode coupling, universality, and the glass transition. Physical Review A, 45, 2393–2398.

Kress, V.C., Williams, Q., and Carmichael, I.S.E. (1988) Ultrasonic investigation of melts in the system Na_2O-Al_2O_3-SiO_2. Geochimica et Cosmochimica Acta, 52, 283–293.

Kubicki, J.D., and Lasaga, A.C. (1988) Molecular dynamics simulations of SiO_2 melt and glass: Ionic and covalent models. American Mineralogist, 73, 941–955.

——— (1990) Molecular dynamics and diffusion in silicate melts. In J. Ganguly, Ed., Diffusion, atomic ordering, and mass transport: Selected problems in geochemistry, p. 1–50. Springer-Verlag, New York.

Kushiro, I. (1983) Effect of pressure on the diffusivity of network-forming cations in melts of jadeitic compositions. Geochimica et Cosmochimica Acta, 47, 1415–1422.

Leutheusser, E. (1984) Dynamical model of the liquid-glass transition. Physical Review A, 29, 2765–2773.

Lewis, L.J. (1991) Atomic dynamics through the glass transition. Physical Review B, 44, 4245–4254.

Liu, S.B., Pines, A., Brandriss, M., and Stebbins, J.F. (1987) Relaxation mechanisms and effects of motion in albite ($NaAlSi_3O_8$) liquid and glass: A high temperature NMR study. Physics and Chemistry of Minerals, 15, 155–162.

Liu, S.-B., Stebbins, J.F., Schneider, E., and Pine, A. (1988) Diffusive motion in alkali silicate melts: An NMR study at high temperature. Geochimica et Cosmochimica Acta, 52, 527–538.

Navrotsky, A. (1994) Repeating patterns in mineral energetics. American Mineralogist, 79, 589–605.

N'Dala, I., Cambier, F., Anseau, M.R., and Urbain, G. (1984) Viscosity of liquid feldspars: I. Viscosity measurements. British Ceramic Transactions and Journal, 83, 105–107.

Oishi, Y., Terai, R., and Ueda, H. (1975) Oxygen diffusion in liquid silicates and relation to their viscosity. In A.R. Cooper and A.H. Heuer, Eds., Mass transport phenomena in ceramics. p. 297–310. Plenum, New York.

Richet, P., and Bottinga, Y. (1984) Glass transitions and thermodynamic properties of amorphous SiO_2, $NaAlSi_nO_{2n+2}$ and $KAlSi_3O_8$. Geochimica et Cosmochimica Acta, 48, 453–470.

Rubie, D.C., Ross, C.R., II, Carroll, M.R., and Elphick, S.C. (1993) Oxygen self-diffusion in $Na_2Si_4O_9$ liquid up to 10 GPa and estimation of high-pressure melt viscosities. American Mineralogist, 78, 574–582.

Rustad, J.R., Yuen, D.A., and Spera, F.J. (1990) Molecular dynamics of liquid SiO_2 under high pressure. Physical Review A, 42, 2081–2089.

Scamehorn, C.A., and Angell, C.A. (1991) Viscosity-temperature relations and structure in fully polymerized aluminosilicate melts from ion dynamics simulations. Geochimica et Cosmochimica Acta, 55, 721–730.

Scherer, G.W. (1986) Relaxation in glasses and composites, 331 p. Wiley, New York.

Seifert, F., Mysen, B.O., and Virgo, D. (1982) Three-dimensional network structure of quenched melts (glass) in the systems SiO_2-$NaAlO_2$, SiO_2-$CaAl_2O_4$ and SiO_2-$MgAl_2O_4$. American Mineralogist, 67, 696–717.

Shimizu, N., and Kushiro, I. (1984) Diffusivity of oxygen in jadeite and diopside melts at high pressures. Geochimica et Cosmochimica Acta, 48, 1295–1303.

Signorini, G.F., Barrat, J.-L., and Klein, M.L. (1990) Structural relaxation and dynamical correlations in a molten state near the liquid-glass transition: A molecular dynamics study. Journal of Chemical Physics, 92, 1294–1303.

Sindzingre, P., and Klein, M.L. (1992) A molecular dynamics study of methanol near the liquid-glass transition. Journal of Chemical Physics, 96, 4681–4692.

Soules, T.F., and Busbey, R.F. (1981) Sodium diffusion in alkali silicate glass by molecular dynamics. Journal of Chemical Physics, 75, 969–975.

Stebbins, J.F., Farnan, I., and Xue, X.Y. (1992) The structure and dynamics of alkali silicate liquids: A view from NMR spectroscopy. Chemical Geology, 96, 371–385.

Stebbins, J.F., George, A.M., and Sen, S. (1994) Alkali cation sites and dynamics in silicate liquids: High temperature NMR spectroscopic results. Eos, 75, 714.

Stein, D.J., and Spera, F.J. (1993) Experimental rheometry of melts and supercooled liquids in the system $NaAlSiO_4$-SiO_2: Implications for structure and dynamics. American Mineralogist, 78, 710–723.

——— (1995) Molecular dynamics simulations of liquids and glasses in the system $NaAlSiO_4$-SiO_2: Methodology and melt structures. American Mineralogist, 80, 417–431.

Stillinger, F.H. (1995) A topographic view of supercooled liquids and glass formation. Science, 267, 1935–1939.

Taylor, M., and Brown, G.E. (1979) Structure of mineral glasses: II. The SiO_2-$NaAlSiO_4$ join. Geochimica et Cosmochimica Acta, 43, 1467–1473.

Terai, R. (1969) Self-diffusion of sodium ions and electrical conductivity in sodium aluminosilicate glasses. Physics and Chemistry of Glasses, 10, 146–152.

Urbain, G., Bottinga, Y., and Richet, P. (1982) Viscosity of liquid silica, silicates and alumino-silicates. Geochimica et Cosmochimica Acta, 46, 1061–1072.

Wahnstrom, G. (1991) Molecular-dynamics study of a supercooled two-component Lennard-Jones system. Physical Review A, 44, 3752–3764.

Wendlandt, R.F. (1991) Oxygen diffusion in basalt and andesite melts: Experimental results and discussion of chemical versus tracer diffusion. Contributions to Mineralogy and Petrology, 108, 463–471.

Woodcock, L.V., Angell, C.A., and Cheeseman, P. (1976) Molecular dynamics studies of the vitreous state: Simple ionic systems and silica. Journal of Chemical Physics, 65, 1565–1577.

Yinnon, H., and Cooper, A.R., Jr. (1980) Oxygen diffusion in multicomponent glass forming silicates. Physics and Chemistry of Glasses, 21, 204–211.

MANUSCRIPT RECEIVED MARCH 30, 1995
MANUSCRIPT ACCEPTED DECEMBER 7, 1995